J. Condensed Matter Nucl. Sci. 13 (2014) 177–222

Research Article

Models for Phonon–nuclear Interactions and Collimated X-ray Emission in the Karabut Experiment

Peter L. Hagelstein *

Research Laboratory of Electronics, Massachusetts Institute of Technology, Cambridge, MA 02139, USA

Irfan U. Chaudhary

Department of Computer Science and Engineering, University of Engineering and Technology. Lahore, Pakistan

Abstract

Excess heat in the Fleischmann–Pons experiment occurs without commensurate energetic nuclear radiation, which motivated us to seek mechanisms capable of fractionating a large quantum, resulting in the lossy spin-boson model. Collimated x-ray emission in the Karabut experiment we interpreted as demonstrating the conversion of vibrational energy to nuclear excitation, as predicted from the lossy spin-boson model; this motivated us to seek physical models that could account for the effect. We found that the coupling strength associated with electron–nuclear and electron–electron coupling was too weak to fractionate keV quanta into 100 MHz vibrations, which motivated us to seek a theory in which nuclear transitions coupled directly to vibrations. These considerations led us to a lattice model with a relativistic description of compound nuclei, in which a strong phonon-nuclear interaction is present. This interaction is normally rotated out with the Foldy–Wouthuysen transformation, but in the presence of strong loss mechanisms this transformation becomes unhelpful. The model that results describes the coupling of vibrational energy to nuclear excitation, but earlier efforts to apply it to the Karabut experiment resulted in inconsistencies. This motivated us to analyze fluctuations due to electron-phonon coupling in metals, which we find here to be a weak effect for Bloch picture phonon exchange, and a somewhat stronger effect with Born–Oppenheimer phonon exchange. As no new physics were found to substantially enhance fractionation, we returned to the basic theory, and carried out a systematic analysis of the three different degrees of freedom that result from simple product approximations for the wavefunction. We find that when there are more virtual phonons than real, a significant enhancement of the coupling strength occurs, corresponding to a new anomalous regime. Conditions on the coupling matrix element and relative state occupation are derived for the anomalous regime, which favors strongly-coupled low energy transitions which constitute a large fraction of all nuclei present. The fractionation power of a sample in the anomalous regime is very much constrained, which allows us to be able to make predictions with the new model. We find that the 30.77 keV transition in ^{93}Nb is likely to be in the anomalous regime in a Nb cathode; that the threshold fractionation energy is too low for excitation of the 30.77 keV transition; but that the threshold fractionation energy is high enough to result in the excitation of the 1565 eV transition in ^{201}Hg, and x-ray emission in the few keV regime consistent with Karabut's observations.
 ISSN 2227-3123

© 2014 ISCMNS. All rights reserved. ISSN 2227-3123

Keywords: Collimated X-rays, Fractionation, Karabut experiment, Phonon–nuclear coupling, Phonon theory

1. Introduction

We have been interested for years in mechanisms by which a large quantum can be fractionated, and quantum systems that exhibit efficient coherent energy exchange under conditions of fractionation. The initial motivation for this came from the excess heat effect in the Fleischmann–Pons experiment [1–3]; in which a great deal of energy is seen which is thought to have a nuclear origin; where ^{4}He has been observed correlated with the excess energy [4–7]; but energetic nuclear radiation is not seen in amounts commensurate with the energy produced [8,9]. As this problem is highly nontrivial, probably the place to start is with simple idealized models in which the mechanism can be studied independently of the distractions associated with a real physical system. For example, in the course of our research we focused on the idealized problem of equivalent two-level systems linearly coupled with an oscillator. The two-level systems in such a model stand in for the nuclear transitions, where the transition energy is large; and the oscillator stands in for a condensed matter degree of freedom, such as a highly excited phonon mode, where the characteristic oscillator energy is much smaller.

This simple idealized model is well studied in the literature [10–12], and it is known as the spin–boson model. Without modification the spin–boson model describes coherent energy exchange between the two-level systems and oscillator when appropriate resonance conditions are satisfied. The basic effect in this model is not particularly strong [13,14]. For example, modest rates for coherent energy exchange are predicted under conditions where the large two-level system quantum is exchanged for tens of oscillator quanta; but unfortunately the model seems to run out of steam under conditions of greater fractionation. We were interested in the question of what limited the effect in the spin-boson model. After some investigation, we found that the problem was that destructive interference limited the rate of coherent energy exchange under conditions of fractionation [15,16]. If we think of it in terms of perturbation theory, coherent energy exchange requires indirect coupling between two nearly-resonant states separated by a large number of intermediate off-resonant states. Contributions to the indirect coupling come from all possible pathways between the two nearly resonant states, of which there are many when a large quantum is fractionated. Some of the contributions come with one sign, and some with another, so that in the end there is exquisite cancellation so that the sum is orders of magnitude smaller than the individual contributions.

In the Brillouin–Wigner formalism [17], loss mechanisms are dependent on how far off of resonance a basis state is. Hence, basis states with much more energy than available to the system see slow or negligible decay rates, while basis states with much less energy than available to the system can see increased decay rates [16]. In the event that decay mechanisms are fast, it is possible for loss to cause some of the off-resonant basis states to have much reduced occupation. The absence of the contribution to the indirect coupling spoils the cancellation effect discussed above, and we find that the resulting indirect coupling can be very strong when such loss is added to the spin–boson model [18–21].

Once this mechanism was understood, our attention turned to the problem of finding a physical system which could support the mechanism, and which had something to do with the anomalies seen in connection with Fleischmann–Pons studies [22]. It turns out that many physical systems are consistent with this fractionation mechanism, and there is no difficulty in arguing that most of the anomalies seen in experiment can be predicted to occur in suitably designed experiments. For example, there are known weak couplings between nuclear transitions and lattice vibrations, and under appropriate conditions there is no difficulty in calculating that large quanta can be fractionated. Such models predict coherent processes in which two deuterons make ^{4}He, with the energy going into vibrations; lattice-induced

*E-mail: plh@mit.edu

nuclear excitation, leading to gamma emission and nuclear disintegration; and lattice-induced nuclear excitation leading to collimated x-ray emission, as seen in the Karabut experiment [23–28]. However, such models are not particularly close to experiment quantitatively. Although anomalies are predicted, the coupling implied in the experiments is orders of magnitude larger than available in the conventional models.

This motivated us to consider unconventional models, which eventually led us to focus on the very strong coupling between vibrations and internal nuclear degrees of freedom present in relativistic models for composite nuclei [29–31]. Normally this strong coupling is eliminated by a generalized Foldy–Wouthuysen transformation, resulting in a dressed picture in which only a very weak residual second-order coupling remains. However, a Foldy–Wouthuysen transformation also eliminates the strong first-order coupling in the spin–boson model [13]. But when loss is present, coherent energy exchange under conditions of fractionation proceeds at a rate determined by the first-order coupling [20]. In a sense, the Foldy–Wouthuysen transformation becomes unhelpful for the lossy spin–boson model, primarily because the transformed loss operator in the rotated picture is large and complicated. In the presence of strong loss, it is simpler not to use the Foldy–Wouthuysen transformation and just analyze the problem in the original unrotated basis.

The resulting phonon–nuclear model is very interesting. As was the case for conventional coupling, this new model predicts coherent energy exchange under conditions of fractionation, which means that pretty much the full array of the anomalies observed in experiment are predicted. To check whether the new theory might have predictive capability, we decided to check against collimated X-ray emission in the Karabut experiment. As remarked upon previously, such a comparison relies on the underlying theory, the interpretation of the experiment, and on the details of the model and model parameters used. Once again we did not obtain consistency between theory and experiment (but things are very much closer than with earlier models before the new relativistic model); a version of this comparison is given below in Section 8. This lack of agreement provided us with motivation in an earlier work [32], and also in this work, to double check issues with the basic theory to see whether something was missing.

The focus of our efforts was on the issue of phonon fluctuations that result from the coupling between vibrations and electrons in a metal. In a sense, coherent energy exchange in the phonon-nuclear model occurs through phonon fluctuations produced as a second-order effect which results from the strong phonon-nuclear coupling (as seen in the

$$\frac{g}{(\Delta n)^2}\frac{\mathrm{d}^2}{\mathrm{d}z^2}$$

term that appears in the continuum model of Ref. [20]). It seems pretty clear in the model that if there are additional mechanisms capable of producing phonon fluctuations, that these might impact coherent energy exchange in the phonon-nuclear model.

As a result of all of this, we became interested in the development of a model for phonon fluctuations in a metal [32]. This problem is easily stated, but very quickly technical issues arise. The problem that we face at the outset has to do with the basic picture (or rather, two basic pictures) of the coupled system of conduction electrons and phonons in the literature. One basic approach to the problem follows from the Born–Oppenheimer approximation, in which the nuclear motion is assumed slow, so that an adiabatic model can be used for the electrons. In the Born–Oppenheimer picture, there is a static screening effect associated with the conduction electrons (that does not involve phonon exchange), and phonon exchange is responsible for dynamical effects at second order and higher. The other basic approach involves the Bloch picture, in which conduction electrons respond to the dynamical motion of the metal ions through phonon exchange. Electron screening in the Bloch picture then comes about as a result of phonon exchange. Over the years there has been occasional discussions about these two pictures [33,34]; nearly all calculations are done in the Bloch picture (because it is much simpler), and it is generally agreed that basic results for screening and phonon decay are the same in the two pictures [35].

The development of a fluctuation model in the Bloch picture is conceptually simple, since we have available explicit expressions for the relevant coupling matrix elements [35,36], and we know how to evaluate the parameters that describe

fluctuations [32]. Fluctuations in the Bloch picture are very strong (we will see in Section 6 that fluctuations due to phonon-nuclear coupling can be stronger still). This can be attributed to how phonon dynamics in the Bloch model come about in the first place. Coulomb repulsion at long wavelength between the ions would result in vibrations at the ion plasma frequency for longitudinal modes, but electron screening in the resonant sector very nearly cancels out this contribution and reduces the vibrational frequency to much lower values. Off of resonance the screening of the electrons is reduced, the lattice stiffens up, and the vibrational frequency increases (approaching the ion plasma frequency if the screening were eliminated completely). In a calculation which is referenced to the phonon mode basis of the resonant sector, we would find little difference in the mode structure in the case of a simple monatomic metal as we go off of resonance; however the frequency changes in the off-resonant sectors, and off-diagonal coupling arises. This gives rise to the phonon fluctuations. A model for these fluctuations is discussed in Sections 2 and 3.

The situation in the Born–Oppenheimer picture at the outset is much less clear, primarily since there has been much less in the way of analysis in this picture to draw from. We know that in the resonant sector the static part of the screening comes about due to conventional interactions with electrons that involves no phonon exchange [32]. Non-adiabatic and phonon exchange contributions in this case results in a weak dynamical correction. It was unclear to us initially how the Born–Oppenheimer version of the model works in the off-resonant sectors. For example, since phonon exchange effects are so weak in the resonant sector, we imagined that the could become even weaker in the off-resonant sectors.

However, by now we have some experience with the Born–Oppenheimer picture (both on and off of resonance), as well as with the Bloch picture. We also know much more about the issues involved in accessing off-resonant states in connection with the phonon-nuclear interaction. We can develop a fluctuation model for this case similarly to the the one for the Bloch picture. In Section 3 we present the results of a calculation of the associated shift for the fixed-point picture, in which the phonon exchange is Born–Oppenheimer. The results are interesting. While the Bloch picture and Born–Oppenheimer picture give similar results in many calculations as mentioned above, for fluctuations the two models give very different results at low frequency. In the Bloch picture, fluctuations are modest in comparison to the nonphysically large fluctuations resulting from the fixed-point formula in the low frequency limit. This motivates us to propose that the validity of the Born–Oppenheimer approximation might be at issue for the slow electrons which dominate the contributions to the fluctuations.

Now that we have a fluctuation model, we can address the question as to whether these fluctuations substantially enhance the ability of the system to fractionate a large quantum. In Section 6 we find that the fluctuations in the Bloch picture have only a small impact in comparison to fluctuations already present due to the strong phonon-nuclear coupling. On the one hand this might be viewed as discouraging, since we had hoped to see an enhancement of fractionation power due to electron–phonon interactions. On the other hand, the fact that electron–phonon interactions make little difference means that the problem simplifies, and that we should consider the phonon–nuclear interaction as a very strong and robust effect in its own right.

Since the inclusion of additional phonon fluctuations in the phonon-nuclear model makes little difference, we are faced once more with the issue of a lack of agreement between theory and experiment in connection with X-ray emission in the Karabut model. We recall that the test involved the underlying theory, the interpretation of the experiment, and the specification of a model and model parameters. As we found no issue with the underlying theory, our attention turns to the interpretation and the associated model. This provides us with the motivation to go back to the basic theory systematically, and more carefully, and see whether something was missed in the earlier models (in Sections 4–7), or perhaps in the interpretation (in Section 8). As will be seen, we have found a new regime in which the model shows an enhanced ability to fractionate large quanta (Sections 7 and 8).

2. Phonon–nuclear Model and Phonon Fluctuations

The addition of a phonon fluctuation model to the phonon–nuclear model is straightforward; however, it seems appropriate here to consider the problem in the context of the reduction from the fundamental Hamiltonian. In previous papers we have considered different parts of this reduction and associated issues in some detail. Rather than reproducing the full calculation, we are then motivated here to develop a shortened version of the development. This will hopefully be useful in providing a distillation of what has come before, and also in providing a foundation for the discussion in the following sections.

While this paper was under development, we had put together a detailed description of the reduction of the second-order phonon exchange contribution for both the diagonal and off-diagonal cases for the fixed-point picture with Born–Oppenheimer phonon exchange [32], and also for the Bloch picture equivalent. For the Bloch picture case, the results were the same for the diagonal case in the resonant sector (which might be thought of as on the mass shell, or involving real states) as appear in the literature. The generalization to the off-resonant case (which correspondingly might be thought of as off the mass shell, or involving virtual states) is trivial, and essentially identical expressions result for the off-diagonal interaction. After some thought, it became clear why this should be so; a force model that is different from the diagonal resonant sector can only come into the problem off of resonance in one way. The frequency shift off of resonance is very closely related to the off-diagonal coupling parameters, which simplifies the model considerably. Once we recognize this, the generalization to a fixed-point model becomes straightforward. Since the fixed-point phonon exchange interaction is so closely related to the Bloch phonon exchange interaction, the same basic approach can be used for either. Because of this, it seemed much less important to include a detailed reduction of the fixed-point interaction, as the end result is reasonably obvious given developments already in the literature. This allows us to focus on the results here, rather on the associated development of the fixed-point expressions.

2.1. Fundamental Hamiltonian

We begin with the fundamental Hamiltonian [29–32]

$$\hat{H} = \sum_j \left(\mathbf{M}c^2 + \mathbf{a}\cdot c\hat{\mathbf{P}} \right)_j + \sum_k \frac{|\hat{\mathbf{p}}_k|^2}{2m} + \sum_{j<j'} \frac{Z_j Z_{j'} e^2}{4\pi\epsilon_0 |\mathbf{R}_{j'} - \mathbf{R}_j|} + \sum_{k<k'} \frac{e^2}{4\pi\epsilon_0 |\mathbf{r}_{k'} - \mathbf{r}_k|} - \sum_{j,k} \frac{Z_j e^2}{4\pi\epsilon_0 |\mathbf{r}_k - \mathbf{R}_j|}. \quad (1)$$

We see a relativistic matrix description for the composite nuclei which includes all rest frame basis state energies in $\mathbf{M}c^2$ (including negative energy states), and all internal transitions due to coupling with the center of mass momentum in the $\mathbf{a}$ matrix. The description of the electronic system here is nonrelativistic. Included are simple Coulomb interactions between nuclei and other nuclei, electrons and other electrons, and between electrons and nuclei. This model provides a direct generalization of the conventional solid-state Hamiltonian to include vibrational coupling between the lattice and internal nuclear degrees of freedom.

2.2. Isolation of the preferred transition

The fundamental Hamiltonian above is very complicated, but it provides us with a more complete description of the nuclear part of the problem. Normally we would make use of a generalized Foldy–Wouthuysen transformation to decouple the vibrations and internal nuclear degrees of freedom [31]

$$\hat{\mathrm{U}}^{\dagger}\left(\mathbf{M}c^2+\mathbf{a}\cdot c\hat{\mathbf{P}}\right)\hat{\mathrm{U}} \;=\; \mathbf{M}c^2\sqrt{1+\frac{|c\hat{\mathbf{P}}|^2}{(\mathbf{M}c)^2}}. \tag{2}$$

We have found that in the presence of strong loss mechanisms (which increase rapidly off of resonance for basis states with less energy than available in the resonant sector), the Foldy–Wouthuysen transformation becomes unhelpful [31]. In this case the rotation still decouples the strong first-order coupling between vibrations and internal nuclear degrees of freedom, but the rotated loss becomes very hard to work with. This was the situation in the case of the spin–boson model, which can be decoupled with a Foldy–Wouthuysen transformation [13]. However, in the presence of strong loss the model behaves differently qualitatively, and it is simplest to simply analyze the problem directly in the unrotated basis [16,18–20].

We now have some experience with this kind of problem in connection with the phonon-nuclear problem under consideration here. What we find is that for most transitions included in the **a** matrix, one arrives at the same answer as would have been obtained had a Foldy–Wouthusyen rotation been used [31]. Even though loss mechanisms makes it so we cannot take advantage of the Foldy–Wouthuysen transformation, it is not easy to arrange for something much different to happen on any particular transition (for example, anomalies are not seen from day to day in mainstream laboratories; and according to the models rather specialized conditions are needed for the coherent dynamics under discussion to occur).

As a result, we would expect coherent dynamics on only a small number of special transitions (those with strong coupling, relatively low transition energy, reasonably stable upper and lower states, with very strong occupation of at least one of the states). All other transitions are benign; consequently it seems a reasonable approximation to isolate the preferred (dynamic) transitions from all of the others (which are static) [31]

$$\mathbf{a} \;\rightarrow\; \mathbf{a}_{\mathrm{static}}+\mathbf{a}_{\mathrm{dynamic}} \tag{3}$$

Since only a tiny part of the **a** matrix is involved in the dynamic transitions, we would expect (and calculations support) that it would be a good approximation (even in the presence of loss) to take

$$\begin{aligned}\hat{\mathrm{U}}^{\dagger}\left(\mathbf{M}c^2+\mathbf{a}_{\mathrm{static}}\cdot c\hat{\mathbf{P}}\right)\hat{\mathrm{U}} \;&\rightarrow\; \mathbf{M}c^2\sqrt{1+\frac{|c\hat{\mathbf{P}}|^2}{(\mathbf{M}c)^2}}\\ &\rightarrow\; \mathbf{M}c^2+\frac{|\hat{\mathbf{P}}|^2}{2\mathbf{M}},\end{aligned} \tag{4}$$

where $\hat{\mathrm{U}}$ is an incomplete Foldy–Wouthuysen transformation (since a few transitions are not included). The idea is that for the static transitions, when we compute the associated occupation, we get the same result we would have gotten in the absence of the loss term that prevents us from exploiting the Foldy–Wouthuysen transformation globally. Hence, it is as if Foldy–Wouthuysen works for all transitions that are not dynamic (an exception to this will be required later in this paper in Section 8 where transitions that make it into an anomalous regime, but are otherwise static, need to be included with the dynamic transitions).

We make use of this argument then to write

$$\hat{H} \rightarrow \sum_j \frac{|\hat{\mathbf{P}}_j|^2}{2\mathbf{M}_j} + \sum_k \frac{|\hat{\mathbf{p}}_k|^2}{2m} + \sum_{j<j'} \frac{Z_j Z_{j'} e^2}{4\pi\epsilon_0 |\mathbf{R}_{j'} - \mathbf{R}_j|} + \sum_{k<k'} \frac{e^2}{4\pi\epsilon_0 |\mathbf{r}_{k'} - \mathbf{r}_k|} - \sum_{j,k} \frac{Z_j e^2}{4\pi\epsilon_0 |\mathbf{r}_k - \mathbf{R}_j|} + \sum_j \left(\mathbf{M}c^2 + \mathbf{a}_{\text{dynamic}} \cdot c\hat{\mathbf{P}} \right)_j . \tag{5}$$

This Hamiltonian in practice is then one that we can work with for analyzing coherent dynamics that result from phonon-nuclear coupling.

2.3. Counter term

We might work with this kind of Hamiltonian under conditions where the transitions that could be dynamic happen to be static (and also in the conventional regime to be described later in Section 7.3 of this paper). In this case we could rotate the interaction out to second order, which would result in a decoupling of the dynamic transitions and leave us with a second-order contribution of the form

$$\hat{\mathrm{U}}^\dagger \left(\mathbf{M}c^2 + \mathbf{a}_{\text{dynamic}} \cdot c\hat{\mathbf{P}} \right) \hat{\mathrm{U}} \rightarrow \mathbf{M}c^2 + \frac{(\mathbf{a}_{\text{dynamic}} \cdot c\hat{\mathbf{P}})^2}{E - \hat{H}} + \cdots \tag{6}$$

This contains the contribution of the dynamic transitions to the kinetic energy. It is the dominant term that is missing in our earlier incomplete Foldy–Wouthuysen transformation. As a result, it seems reasonable to subtract it out in the Hamiltonian if we are interested in studying the system right when it begins to become dynamic

$$\hat{H} \rightarrow \sum_j \frac{|\hat{\mathbf{P}}_j|^2}{2\mathbf{M}_j} + \sum_k \frac{|\hat{\mathbf{p}}_k|^2}{2m} + \sum_{j<j'} \frac{Z_j Z_{j'} e^2}{4\pi\epsilon_0 |\mathbf{R}_{j'} - \mathbf{R}_j|} + \sum_{k<k'} \frac{e^2}{4\pi\epsilon_0 |\mathbf{r}_{k'} - \mathbf{r}_k|} - \sum_{j,k} \frac{Z_j e^2}{4\pi\epsilon_0 |\mathbf{r}_k - \mathbf{R}_j|} + \sum_j \left[\mathbf{M}c^2 + \mathbf{a}_{\text{dynamic}} \cdot c\hat{\mathbf{P}} - \frac{(\mathbf{a}_{\text{dynamic}} \cdot c\hat{\mathbf{P}})^2}{E - \hat{H}} \right]_j . \tag{7}$$

The counter term here is equivalent to what we have discussed previously in [30,31]. From experience we have had with this kind of model, we know that the counter term is very small compared to the first-order coupling term under conditions where the system undergoes coherent dynamics. So good results can be obtained for rate estimates away from threshold if the counter term is not included.

2.4. Phonons and conduction electrons in the resonant sector

Next we consider the electronic and vibrational degrees of freedom. In the case of a metal the problem has been well-studied studied, and we know that it is possible to work with a dressed system in which the electronic and vibrational degrees of freedom are approximately separated [35–37]. We indicate this by writing

$$\sum_j \frac{|\hat{\mathbf{P}}_j|^2}{2M_j} + \sum_k \frac{|\hat{\mathbf{p}}_k|^2}{2m} + \sum_{j<j'} \frac{Z_j^* Z_{j'}^* e^2}{4\pi\epsilon_0 |\mathbf{R}_{j'} - \mathbf{R}_j|} + \sum_{k<k'} \frac{e^2}{4\pi\epsilon_0 |\mathbf{r}_{k'} - \mathbf{r}_k|} - \sum_{j,k} \frac{Z_j^* e^2}{4\pi\epsilon_0 |\mathbf{r}_k - \mathbf{R}_j|}$$
$$\rightarrow \sum_{\mathbf{q},s} \hbar\omega_{\mathbf{q},s} \left(\hat{a}^\dagger_{\mathbf{q},s} \hat{a}_{\mathbf{q},s} + \frac{1}{2} \right) + \sum_{\mathbf{k},\sigma} E(\mathbf{k}) \hat{c}^\dagger_{\mathbf{k},\sigma} \hat{c}_{\mathbf{k},\sigma} . \tag{8}$$

We will use this for the resonant sector, as there can be a modification of the vibrational frequencies for a highly excited mode off of resonance.

From earlier work we know that coherent dynamics are unlikely to develop as a result of thermal excitation of a phonon bath; in general highly excited (nonthermal) phonon modes are required. Our work has focused so far on models where a single highly excited phonon mode interacts with a few dynamical transitions; consequently, we will isolate a single highly excited phonon mode according to

$$\sum_{\mathbf{q},s} \hbar\omega_{\mathbf{q},s} \left(\hat{a}^\dagger_{\mathbf{q},s} \hat{a}_{\mathbf{q},s} + \frac{1}{2} \right) \rightarrow \hbar\omega_0 \left(\hat{a}^\dagger \hat{a} + \frac{1}{2} \right) + \sum_{\mathbf{q}',s'} \hbar\omega_{\mathbf{q}',s'} \left(\hat{a}^\dagger_{\mathbf{q}',s'} \hat{a}_{\mathbf{q}',s'} + \frac{1}{2} \right) \tag{9}$$

As the other phonon modes have so far not played a role in the coherent dynamics, we can take them to be unexcited or thermal as we wish.

2.5. Frequency shift off of resonance and phonon fluctuations

Because the Foldy–Wouthuysen transformation is unhelpful for analyzing coherent dynamics, we need to model this part of the problem in an unrotated basis. Since the coupling is strong in general, we end up coupling to a great many states that are far off of resonance. At issue then is what changes are needed in the off-resonant sectors.

In a metal, the conduction electrons screen the interaction between the ions. Since the conduction electrons constitute an independent quantum mechanical system, the part of the interaction associated with dynamical screening will change off of resonance, which will result in a change in the phonon frequency off of resonance. Associated with the frequency changes will be corresponding terms that create and destroy phonons, which results in phonon fluctuations. We have been very interested in these phonon fluctuations, as we had hoped that they would produce an enhancement in the ability of the phonon–nuclear system to fractionate a large quantum (we will see that only a small effect results from this).

At issue then is the frequency shift of the highly-excited phonon mode off of resonance, which we will denote through

$$\omega_0 \rightarrow \omega_0(E_{\text{off}}), \tag{10}$$

where E_{off} is the amount of off-resonant energy per phonon in the highly excited phonon mode relative to the resonant sector (with a sign defined to be positive for basis states with more energy than in the resonant sector). There is a technical issue involved here as to how to deal with the off-resonant energy in connection with the phonon frequency. The argument we have relied on is one that makes use of a configuration space picture for individual phonons, with a corresponding optimization for each phonon individually. In this kind of picture on average the total off-resonant energy will be divided up between them, so that the frequency shift will be determined by how far off of resonance a single phonon is.

We will take the contribution of this frequency shift to the Hamiltonian to be

$$\hbar\omega_0\left(\hat{a}^\dagger\hat{a}+\frac{1}{2}\right) \;\rightarrow\; \hbar\omega_0\left(\hat{a}^\dagger\hat{a}+\frac{1}{2}\right)+\frac{1}{2}\hbar\Delta\omega_0(E_{\rm off})\left(\hat{a}^\dagger+\hat{a}\right)^2. \tag{11}$$

This kind of a model is consistent with a force constant model that changes off of resonance

$$\frac{1}{2}\sum_j\sum_k(\mathbf{R}_j-\mathbf{R}_j^{(0)})\cdot\mathbf{K}\cdot(\mathbf{R}_k-\mathbf{R}_k^{(0)}) \;\rightarrow\; \frac{1}{2}\sum_j\sum_k(\mathbf{R}_j-\mathbf{R}_j^{(0)})\cdot\mathbf{K}(E_{\rm off})\cdot(\mathbf{R}_k-\mathbf{R}_k^{(0)}), \tag{12}$$

where $\mathbf{K}$ is a force matrix (and where the force matrix indices are suppressed). If we choose to define the phonon basis based on $\mathbf{K}$ in the resonant sector, then the interaction off of resonance will be

$$\hat{H}_{\rm int}(E_{\rm off}) \;=\; \frac{1}{2}\sum_j\sum_k(\mathbf{R}_j-\mathbf{R}_j^{(0)})\cdot[\mathbf{K}(E_{\rm off})-\mathbf{K}]\cdot(\mathbf{R}_k-\mathbf{R}_k^{(0)}), \tag{13}$$

Once again there are technical issues; however, if we make use of phonon modes defined in the off-resonant sectors, then for the highly excited mode we may write

$$\frac{1}{2}\sum_j\sum_k(\mathbf{R}_j-\mathbf{R}_j^{(0)})\cdot[\mathbf{K}(E_{\rm off})-\mathbf{K}]\cdot(\mathbf{R}_k-\mathbf{R}_k^{(0)}) \;\rightarrow\; \frac{1}{2}\hbar\Delta\omega_0(E_{\rm off})\left(\hat{a}^\dagger+\hat{a}\right)^2. \tag{14}$$

Of interest in connection with this argument is that the phonon fluctuations are connected with the frequency shift. Although at this point there is no problem in calculating the frequency shift, or the dynamical change in the force constant, conceptually it is much simpler to focus on (and to estimate) the frequency shift. Because of this close connection between the frequency shift and the fluctuations, we understand that any vibrating system in which the frequency shifts off of resonance will also have fluctuations. Hence, there is no reason to believe that the fluctuations under discussion for a metal here would be absent in an insulator.

In a strict fixed-point model, the interaction is mediated by momentum operators rather than position operators. In this case, we would use instead

$$\frac{1}{2}\sum_j\sum_k\hat{\mathbf{P}}_j\cdot[\mathbf{L}(E_{\rm off})-\mathbf{L}]\cdot\hat{\mathbf{P}}_k \;\rightarrow\; \frac{1}{2}\hbar\Delta\omega_0(E_{\rm off})\left(\frac{\hat{a}-\hat{a}^\dagger}{i}\right)^2, \tag{15}$$

where the $\mathbf{L}$ matrix is discussed in [32]. This will result in a sign change in the off-diagonal terms.

We note that there is yet another subtle issue in all of this. We are using a model in which the off-resonant energy is divided among the different phonons in the highly excited mode to produce the frequency shift. There may be thermal phonons, so the question might arise as to whether the off-resonant energy should also be shared among them as well. We might go further and point out that there are also conduction electrons which might also be considered as candidates. From our perspective, in connection with coherent dynamics associated with phonon–nuclear interactions, what contributes to the effect are interactions between the highly excited phonon mode and the nuclear system; consequently, the thermal phonon modes are independent degrees of freedom that are not involved (and hence out of the picture for practical purposes). The same can be said of the conduction electrons, once the dynamic response (which comes about from the response of the electrons to the highly excited phonon mode) has been extracted.

2.6. Loss

We first introduced (our version of) the lossy spin–boson model by augmenting the lossless spin–boson model with a Brillouin-Wigner loss operator [16]. The empirical loss added to the model was intended to account for the myriad of fast loss mechanisms (electron promotion, atomic displacement/ejection, and nuclear loss channels) available when a large quantum of excess off-resonant energy became available.

Now that we have a physical model for the system, it is possible for the loss terms to be developed directly from the model (instead of adding them empirically). Consider for example the specific case of phonon loss due to electron promotion. Since our model includes electron-phonon interactions, it also includes this phonon loss channel. In the fixed-point picture [32] we can determine the phonon loss in the resonant sector that results from second-order phonon exchange from

$$-\frac{\hbar}{2}\hat{\Gamma}(E) \;=\; \mathrm{Im}\langle n| - \sum_j \sum_k \hat{\mathbf{P}}_j \cdot \left\{ \sum_{X\neq 0} \frac{\hbar^2}{M_j M_k} \frac{\langle \Phi_0|\nabla_j \Phi_X\rangle_0 \langle \Phi_X|\nabla_k \Phi_0\rangle_0}{E-\hat{H}} \right\} \cdot \hat{\mathbf{P}}_k |n\rangle, \tag{16}$$

where the denominator here is understood to keep track of phonon and electron energies appropriately. In a more general (complex) computation of the phonon mode frequencies that included the imaginary parts of the transformed generalized force matrix, the resulting frequency would be complex. In this case we could determine the loss numerically on resonance from

$$-\frac{1}{2}\Gamma \;=\; n_0 \mathrm{Im}\{\omega_0\}. \tag{17}$$

Off of resonance for basis states with higher energy than the resonant sector, it would probably make sense to compute loss rates with the off-resonant energy spread over all of the phonons, as was discussed for the frequency shift above. Since the frequency shift can be thought of as an average quantity (averaged over all phonons), making use of the per phonon energy deficit seems reasonable. Loss in the presence for resonance states with an energy deficit can probably be thought of similarly, since an energy deficit results in a net reduction of the loss rate. However, in the case of an energy surplus (where the basis states have less energy than available in the resonant sector), the system would be able to make a transition to a final state in the (post-loss) resonant sector by losing the excess energy. Hence, there is a net benefit for the system in exchanging substantial excess energy in a single loss for these basis states, rather than spreading the excess energy over all phonons. In this case we could make use of an appropriate off-resonant version of Eq. (16) to compute the associated (very fast) decay rate. As discussed above, such fast loss can reduce state occupation where an energy excess is present, which makes the problem behave qualitatively differently. In future work it will be of interest to revisit the estimation of decay rates based on realistic models.

We have argued that the Foldy–Wouthuysen transformation becomes unhelpful in the presence of fast decay mechanisms that reduces or eliminates occupation of basis states needed for the rotation [31]. In essence a generalized Foldy–Wouthuysen transformation of the loss turns into a complicated operator that is very hard to deal with. We have such an example here already in Eq. (16). In the unrotated problem with strong coupling, we have a wide range of basis states involved; some with weak decay rates, and some with very fast decay rates. Whether a decay rate is fast or slow depends on the energy offset from resonance. There is no good way to keep track of the states that are unoccupied because of loss in a Foldy–Wouthuysen transformation. This is the reason that the transformation becomes unhelpful in this situation.

2.7. Reduced models

If we make use of the various simplifications above, then the model under consideration can be written as

$$\hat{H} \;\rightarrow\; \hbar\omega_0\left(\hat{a}^\dagger\hat{a}+\frac{1}{2}\right)+\frac{1}{2}\hbar\Delta\omega_0(E_{\rm off})\left(\hat{a}^\dagger+\hat{a}\right)^2+\sum_{\mathbf{q}',s'}\hbar\omega_{\mathbf{q}',s'}\left(\hat{a}^\dagger_{\mathbf{q}',s'}\hat{a}_{\mathbf{q}',s'}+\frac{1}{2}\right)$$
$$+\sum_{\mathbf{k},\sigma}E(\mathbf{k})\hat{c}^\dagger_{\mathbf{k},\sigma}\hat{c}_{\mathbf{k},\sigma}+\sum_j\left[\mathbf{M}c^2+\mathbf{a}_{\rm dynamic}\cdot c\hat{\mathbf{P}}-\frac{(\mathbf{a}_{\rm dynamic}\cdot c\hat{\mathbf{P}})^2}{E-\hat{H}}\right]_j-i\frac{\hbar}{2}\hat{\Gamma}(E). \tag{18}$$

Since the coherent dynamics of interest here do not involve electron promotion (beyond that included in the loss term), there is little reason to retain conduction electrons in the model. Similarly, we are not including interactions with the unexcited or thermal phonon modes, so we will not keep them in our model.

We have already presumed that the nuclear masses are well approximated by the ground state mass in connection with the kinetic energy

$$\frac{|\hat{\mathbf{P}}_j|^2}{2\mathbf{M}_j}\;\rightarrow\;\frac{|\hat{\mathbf{P}}_j|^2}{2M_j}, \tag{19}$$

when we introduced the phonon modes above. However, this model contains a large mass matrix with far more information (about all of the rest frame states) than we require. All we really need is a description of the masses of the states which participate in the coherent dynamics. Hence, we can reduce in this case to

$$\mathbf{M}_j\;\rightarrow\;\begin{cases}M_j & \text{if no coherent dynamics}\\ \text{smaller }\mathbf{M}_j & \text{if coherent dynamics.}\end{cases} \tag{20}$$

There is also no reason to keep the rest masses in the Hamiltonian, as they simply contribute a large constant offset (but do not impact the dynamics).

After all of this, the model that remains can be written as

$$\hat{H} \;\rightarrow\; \hbar\omega_0\left(\hat{a}^\dagger\hat{a}+\frac{1}{2}\right)+\frac{1}{2}\hbar\Delta\omega_0(E_{\rm off})\left(\hat{a}^\dagger+\hat{a}\right)^2-i\frac{\hbar}{2}\hat{\Gamma}(E)$$
$$+\sum_j\left[\mathbf{M}c^2+\mathbf{a}_{\rm dynamic}\cdot c\hat{\mathbf{P}}-\frac{(\mathbf{a}_{\rm dynamic}\cdot c\hat{\mathbf{P}})^2}{E-\hat{H}}\right]_j. \tag{21}$$

This model could reasonably be taken as the starting point for future analyses of anomalies in condensed matter nuclear science. Even though it is much simpler than where we started, the physics in this model is very rich. This model can be used for example to describe coherent dynamics and fractionation involving multiple transitions with spatial nonuniformity, which is likely to include most problems of interest well into the future.

2.8. Uniform interaction and two-level systems

Although much simpler than what we started with, this model is still extremely complicated. We would like to develop even simpler models that can be analyzed more easily. Consequently, the final step in our reduction is to assume a uniform interaction, so that

$$\hat{\mathbf{P}} \;\rightarrow\; \frac{\mathrm{d}\mathbf{P}}{\mathrm{d}a}\left(\frac{\hat{a}-\hat{a}^\dagger}{i}\right) \tag{22}$$

and to assume that only two levels are involved so that

$$\sum_j \left[\mathbf{a}_{\mathrm{dynamic}}\cdot c\hat{\mathbf{P}}\right] \;\rightarrow\; \sum_j \begin{pmatrix} 0 & \mathbf{a} \\ \mathbf{a} & 0 \end{pmatrix}_j \cdot \frac{\mathrm{d}\,\mathbf{P}}{\mathrm{d}a}\left(\frac{\hat{a}-\hat{a}^\dagger}{i}\right)$$

$$= \mathbf{a}\cdot c\frac{\mathrm{d}\,\mathbf{P}}{\mathrm{d}a}\frac{2\hat{S}_x}{\hbar}\left(\frac{\hat{a}-\hat{a}^\dagger}{i}\right). \tag{23}$$

In the last line we make use of a pseudo-spin notation

$$\hat{S}_x \;=\; \frac{\hbar}{2}\sum_j \begin{pmatrix} 0 & 1 \\ 1 & 0 \end{pmatrix}_j . \tag{24}$$

There is a notational issue in that previously **a** was used to describe a very large matrix of vectors, and now **a** is a single vector matrix element for a single nuclear transition. For the mass matrix contribution, we can write

$$\sum_j \mathbf{M}c^2 \;\rightarrow\; \Delta Mc^2 \sum_j \begin{pmatrix} 1/2 & 0 \\ 0 & -1/2 \end{pmatrix}_j$$

$$= \Delta Mc^2 \frac{\hat{S}_z}{\hbar}, \tag{25}$$

where

$$\hat{S}_z \;=\; \frac{\hbar}{2}\sum_j \begin{pmatrix} 1 & 0 \\ 0 & -1 \end{pmatrix}_j . \tag{26}$$

The model that results is

$$\hat{H} \;\rightarrow\; \Delta Mc^2\frac{\hat{S}_z}{\hbar} + \mathbf{a}\cdot c\frac{\mathrm{d}\,\mathbf{P}}{\mathrm{d}a}\frac{2\hat{S}_x}{\hbar}\left(\frac{\hat{a}-\hat{a}^\dagger}{i}\right) + \hbar\omega_0\left(\hat{a}^\dagger\hat{a}+\frac{1}{2}\right) + \frac{1}{2}\hbar\Delta\omega_0(E_{\mathrm{off}})\left(\hat{a}^\dagger+\hat{a}\right)^2$$
$$- i\frac{\hbar}{2}\hat{\Gamma}(E). \tag{27}$$

The counter term is suppressed here. We recognize this as a lossy spin–boson model augmented with phonon fluctuations.

2.9. Basic lossy-spin boson model

As we will see in what follows, the impact of the phonon fluctuations due to electron-phonon coupling is minor, so one could reasonably neglect them resulting in the basic lossy-spin boson model [16]

$$\hat{H} \;\rightarrow\; \Delta M c^2 \frac{\hat{S}_z}{\hbar} + \mathbf{a}\cdot c\frac{\mathrm{d}\,\mathbf{P}}{\mathrm{d}a}\frac{2\hat{S}_x}{\hbar}\left(\frac{\hat{a}-\hat{a}^\dagger}{i}\right) + \hbar\omega_0\hat{a}^\dagger\hat{a} - i\frac{\hbar}{2}\hat{\Gamma}(E). \tag{28}$$

This model is perhaps the simplest to describe coherent energy exchange between nuclear and vibrational degrees of freedom. As we have remarked upon previously, the augmentation of the basic spin–boson model with appropriate loss results in efficient coherent energy exchange under conditions of fractionation.

3. Fluctuation Model for Long Wavelength Phonons

In order to evaluate the impact of phonon fluctuations on the phonon–nuclear problem, we require a model for the associated fluctuation parameters. From the discussion of the previous section we understand that this is equivalent to determining the frequency shift off of resonance. This motivates us to pursue the problem here.

As it turns out, models for vibrations in metals are much simpler for long wavelength phonons, since in this limit the interaction between conduction electrons and ions is "softer" so that a simple Coulomb interaction becomes appropriate. For shorter wavelength phonons, interactions at short range are important so we would require a more accurate pseudo-potential description.

3.1. Bloch picture frequency shift

The simplest place to start is with the Bloch picture, where the acoustic frequency for a monatomic simple metal lattice can be written as [37]

$$\omega_0(E_{\rm off}) \;=\; \omega_i\sqrt{\frac{\epsilon_0}{\epsilon(\mathbf{q},\omega_0 - E_{\rm off}/\hbar)}}, \tag{29}$$

where the ion plasma frequency satisfies

$$\omega_i^2 \;=\; \frac{(Z^*e)^2}{\epsilon_0 N M}. \tag{30}$$

For small excursions off of resonance we can use a Taylor series to write

$$\omega_0(E_{\rm off}) \;=\; \omega_0 + E_{\rm off}\left[\frac{\mathrm{d}}{\mathrm{d}E}\omega_0(E)\right]_{E=0} + \cdots \tag{31}$$

The first derivative can be evaluated to give

$$\begin{aligned}\frac{\mathrm{d}}{\mathrm{d}E}\omega_0(E) \;&=\; -\frac{1}{2}\omega_i\frac{\epsilon_0^{1/2}}{[\epsilon(\mathbf{q},\omega_0 - E/\hbar)]^{\frac{3}{2}}}\frac{\mathrm{d}}{\mathrm{d}E}\epsilon(\mathbf{q},\omega_0 - E/\hbar)\\ &=\; -\frac{1}{2}\omega_0(E)\frac{1}{\epsilon(\mathbf{q},\omega_0 - E/\hbar)}\frac{\mathrm{d}}{\mathrm{d}E}\epsilon(\mathbf{q},\omega_0 - E/\hbar).\end{aligned} \tag{32}$$

To lowest order the frequency shift is

$$\Delta\omega(E_{\rm off}) \;=\; \omega_0(E_{\rm off}) - \omega_0$$
$$\rightarrow \;\; -\frac{1}{2}\left\{\omega_0(E)\frac{1}{\epsilon(\mathbf{q},\,\omega_0 - E/\hbar)}\frac{\rm d}{{\rm d}E}\epsilon(\mathbf{q},\,\omega_0 - E/\hbar)\right\}_{E=0} E_{\rm off}. \tag{33}$$

The relative frequency shift can be expressed as

$$\frac{\Delta\omega(E_{\rm off})}{\omega_0} \;\rightarrow\; -\frac{1}{2}\left\{\frac{\rm d}{{\rm d}E}\ln\epsilon(\mathbf{q},\,\omega_0 - E/\hbar)\right\}_{E=0} E_{\rm off}. \tag{34}$$

3.2. Longitudinal dielectric constant

In the random phase approximation, the longitudinal dielectric constant for a simple plane wave model for the electrons can be written as

$$\frac{\epsilon(\mathbf{q},\,\omega)}{\epsilon_0} \;=\; 1 - \sum_{\mathbf{k},\sigma}\frac{2e^2}{\epsilon_0 V|\mathbf{q}|^2}\frac{n_F(\mathbf{k})[1-n_F(\mathbf{k}+\mathbf{q})]}{\hbar\omega + E(\mathbf{k}) - E(\mathbf{k}+\mathbf{q})}. \tag{35}$$

We can write this in a continuum approximation as

$$\frac{\epsilon(\mathbf{q},\,\omega)}{\epsilon_0} \;=\; 1 + \frac{4e^2}{\epsilon_0|\mathbf{q}|^2}\int\frac{n_F(\mathbf{k})[1-n_F(\mathbf{k}+\mathbf{q})]}{E(\mathbf{k}+\mathbf{q}) - E(\mathbf{k}) - \hbar\omega}\frac{{\rm d}\mathbf{k}^3}{(2\pi)^3}. \tag{36}$$

If we take the $T = 0$ limit, we may write

$$\frac{\epsilon(\mathbf{q},\,\omega)}{\epsilon_0} \;\rightarrow\; 1 + \frac{4e^2}{\epsilon_0|\mathbf{q}|^2}\frac{1}{(2\pi)^2}\frac{k_F^3}{E_F}\int_{-1}^{1}{\rm d}x\int_0^1\kappa^2{\rm d}\kappa\left\{\frac{\Theta(\sqrt{\kappa^2+\eta^2+2\kappa\eta x}-1)}{\eta^2+2\kappa\eta x-\Omega}\right\}, \tag{37}$$

where

$$\kappa \;=\; \frac{|\mathbf{k}|}{k_F}, \qquad \eta \;=\; \frac{|\mathbf{q}|}{k_F}, \qquad \Omega \;=\; \frac{\hbar\omega}{E_F}. \tag{38}$$

From direct numerical computations for a model for long wavelength vibrations in Na (as a representative metal often used for this kind of model), we can estimate

$$\left\{\frac{\rm d}{{\rm d}E}\ln\epsilon(\mathbf{q},\,\omega_0 - E/\hbar)\right\}_{E=0} \;\rightarrow\; -\frac{0.013}{\hbar\omega_0}. \tag{39}$$

The numerical parameter in this formula depends on the Fermi energy E_F, the Fermi wave vector k_F, and the effective mass of the electrons in this model; consequently we expect similar values for other metals. This result, combined with the relative frequency shift of Eq. (34) is sufficient to specify a fluctuation model.

3.3. Frequency shift in the fixed-point picture

Perhaps the simplest way to make progress toward a fixed-point picture calculation is to go back to the dispersion relation calculation in the Bloch picture, and write it as

$$\begin{aligned}\omega_0^2 &= \frac{\omega_i^2}{\epsilon_0}\left[1-\frac{\epsilon(\mathbf{q},\omega)-\epsilon_0}{\epsilon(\mathbf{q},\omega)}\right]_{\omega=-\omega_0} \\ &= \frac{\omega_i^2}{\epsilon_0}\left[1+\frac{\pi(\mathbf{q},\omega)}{\epsilon(\mathbf{q},\omega)}\right]_{\omega=-\omega_0}\end{aligned} \tag{40}$$

with

$$\frac{\pi(\mathbf{q},\omega)}{\epsilon_0} = \sum_{\mathbf{k},\sigma}\frac{2e^2}{\epsilon_0 V|\mathbf{q}|^2}\frac{n_F(\mathbf{k})[1-n_F(\mathbf{k}+\mathbf{q})]}{\hbar\omega+E(\mathbf{k})-E(\mathbf{k}+\mathbf{q})} \qquad \text{(Bloch)}. \tag{41}$$

The interpretation here is that π in this model is associated with the ion–electron interaction, and ϵ is associated with the screening by the conduction electrons.

In the fixed-point picture phonon exchange between the electrons and ions works differently (as appropriate for a Born–Oppenheimer picture), which we can take into account for long wavelengths in the phonon exchange contribution through

$$\frac{\pi(\mathbf{q},\omega)}{\epsilon_0} = \sum_{\mathbf{k},\sigma}\frac{2e^2}{\epsilon_0 V|\mathbf{q}|^2}\frac{(\hbar\omega_0)^2 n_F(\mathbf{k})[1-n_F(\mathbf{k}+\mathbf{q})]}{[E(\mathbf{k})-E(\mathbf{k}+\mathbf{q})]^2[\hbar\omega+E(\mathbf{k})-E(\mathbf{k}+\mathbf{q})]} \qquad \text{(Fixed}-\text{point)}. \tag{42}$$

We cannot make use of the phonon exchange contribution in the fixed-point model to determine the phonon frequency as in the Bloch picture, but there is no difficulty in using the phonon exchange contribution to estimate the frequency shift. To lowest order we may write

$$2\omega_0\Delta\omega = \frac{\omega_i^2}{\epsilon_0}\left[\frac{\mathrm{d}}{\mathrm{d}E}\frac{\pi(\mathbf{q},\omega_0-E/\hbar)}{\epsilon(\mathbf{q},\omega_0-E/\hbar)}\right]_{E=0}\Delta E_{\mathrm{off}}. \tag{43}$$

This can be rewritten as

$$\frac{\Delta\omega}{\omega_0} = \frac{1}{2}\frac{\epsilon(\mathbf{q},\omega_0)}{\epsilon_0}\left[\frac{\mathrm{d}}{\mathrm{d}E}\frac{\pi(\mathbf{q},\omega_0-E/\hbar)}{\epsilon(\mathbf{q},\omega_0-E/\hbar)}\right]_{E=0}\Delta E_{\mathrm{off}}. \tag{44}$$

The evaluation of this derivative is made complicated by the fact that the continuum integral is (logarithmically) singular. If we assume that the lowest compressional mode of a plate is highly excited (and use an appropriate cut-off), then over a modest range of long wavelength modes (around $\eta = 10^{-2}$) we can estimate from numerical calculations for Na

$$\frac{\epsilon(\mathbf{q},0)}{\epsilon_0}\left[\frac{\mathrm{d}}{\mathrm{d}E}\frac{\pi(\mathbf{q},-E/\hbar)}{\epsilon(\mathbf{q},-E/\hbar)}\right]_{E=0} \rightarrow \left(\frac{0.000234\ \mathrm{eV}}{\hbar\omega_0}\right)^4\frac{1}{\hbar\omega_0}. \tag{45}$$

We conclude that phonon fluctuations can be much larger at long wavelengths in the fixed-point model.

3.4. Discussion

As we can see from the discussion above, one expects a different frequency shift off of resonance in the Bloch picture versus the Born–Oppenheimer based fixed-point picture. In the literature the Bloch picture and Born–Oppenheimer pictures give similar answers for most problems that have been studied; here we get a qualitatively different behavior.

Our intuition suggests that the Bloch picture with the low fluctuations is appropriate for a macroscopic sized metal at long wavelengths, and that Born–Oppenheimer picture is probably inappropriate in this regime (in connection with fluctuations). At this point it may be useful to think a bit about the adiabatic approximation itself. The premise of the Born–Oppenheimer approximation is that the nuclear velocity is slow compared to the electron velocity, so that the use of electronic wavefunctions determined with fixed nuclei is sensible. However, in the simple models under discussion here, the relevant velocity in the longitudinal wave direction is the compressional sound speed c_L. If the sample is large, then there are many electrons that contribute with electron velocities in the same direction less than the compressional sound speed. It is not difficult to imagine that the Born–Oppenheimer approximation is ill-suited for these electrons.

We could imagine working with a thin film for which localization due to the film boundaries would eliminate these slow electrons. We could estimate the plate thickness at threshold from

$$v \;=\; \frac{\hbar k}{m^*} \;\rightarrow\; \frac{\hbar \pi}{m^* L} \;=\; c_L. \tag{46}$$

The lowest phonon frequency at this threshold would satisfy

$$\hbar\omega_0 \;=\; \hbar c_L \frac{\pi}{L} \;=\; m^* c_L^2. \tag{47}$$

For Na, the threshold thin film thickness is about 1000 Å, and the threshold phonon energy is about 60 μeV. For example, if we were to require that this threshold be exceeded by an order of magnitude or so, then the relative shift consistent with Eq. (45) would be plausible.

Consequently, we can imagine that compressional vibrations in a nano-scale metal sample could be reasonably described within a Born–Oppenheimer type of picture. Thicker samples that are 1μ or greater are probably well described using a Bloch picture for long wavelength acoustic phonons. From this point of view, the appearance of a characteristic energy in the fixed point formula for the relative frequency shift is then not surprising. When the phonon energy gets to be much less than the characteristic energy, which is where the frequency shift becomes anomalously large, the Born–Oppenheimer approximation itself may well be inappropriate.

4. Local Approximation

Our attention now returns to the coupled phonon–nuclear model, which now includes an additional term that accounts for phonon fluctuations. We are interested in developing approximate solutions for eigenfunctions of the model, and ultimately to determine the rate of coherent energy exchange under conditions of fractionation. In previous work we have analyzed very similar models, so we we can take advantage of this earlier analysis for this model. The basic idea is that when n is very large, we can analyze the rate at which coherent energy exchange occurs by working with a periodic approximation in n and m space [19].

4.1. Finite basis approximation

We are interested in developing approximate solutions for the time-independent Schrödinger equation

$$E\Psi \;=\; \left\{\Delta Mc^2\frac{\hat{S}_z}{\hbar}+\left(\mathbf{a}\cdot c\frac{\mathrm{d}\mathbf{P}}{\mathrm{d}a}\right)\frac{\hat{S}_x}{2\hbar}\left(\frac{\hat{a}-\hat{a}^\dagger}{i}\right)+\hbar\omega_0\left(\hat{a}^\dagger\hat{a}+\frac{1}{2}\right)+\frac{\hbar\Delta\omega(E)}{2}\left(\hat{a}^\dagger+\hat{a}\right)^2-i\frac{\hbar}{2}\hat{\Gamma}(E)\right\}\Psi. \quad (48)$$

We make use of a finite basis approximation of the form

$$\Psi \;=\; \sum_m\sum_n \mathrm{e}^{i\frac{\pi}{2}n}c_{m,n}|S,m\rangle|n\rangle. \quad (49)$$

The expansion coefficients then satisfy an eigenvalue equation of the form

$$\begin{aligned}Ec_{m,n} \;=\; &\left\{\Delta Mc^2m+\hbar\Big[\omega_0+\Delta\omega(E)\Big]\left(n+\frac{1}{2}\right)-i\frac{\hbar}{2}\Gamma(E)\right\}c_{m,n}\\ &+\left(\mathbf{a}\cdot c\frac{\mathrm{d}\mathbf{P}}{\mathrm{d}a}\right)\sqrt{(S-m)(S+m+1)}\Big[\sqrt{n+1}c_{m+1,n+1}+\sqrt{n}c_{m+1,n-1}\Big]\\ &+\left(\mathbf{a}\cdot c\frac{\mathrm{d}\mathbf{P}}{\mathrm{d}a}\right)\sqrt{(S+m)(S-m+1)}\Big[\sqrt{n+1}c_{m-1,n+1}+\sqrt{n}c_{m-1,n-1}\Big]\\ &-\frac{1}{2}\hbar\Delta\omega(E)\Big[\sqrt{(n+2)(n+1)}c_{m,n+2}+\sqrt{n(n-1)}c_{m,n-2}\Big].\end{aligned} \quad (50)$$

4.2. Approximate form

As before we will assume that

$$n \;\gg\; 1 \quad (51)$$

and also that

$$|S\pm m| \gg 1. \quad (52)$$

In this case the eigenvalue equation is approximated by

$$\begin{aligned}Ec_{m,n} \;=\; &\left\{\Delta Mc^2m+\hbar\Big[\omega_0+\Delta\omega(E)\Big]n-i\frac{\hbar}{2}\Gamma(E)\right\}c_{m,n}-\frac{n}{2}\hbar\Delta\omega(E)\Big[c_{m,n+2}+c_{m,n-2}\Big]\\ &+\frac{1}{i}\left(\mathbf{a}\cdot c\frac{\mathrm{d}\mathbf{P}}{\mathrm{d}a}\right)\sqrt{n}\sqrt{S^2-m^2}\Big[c_{m+1,n+1}-c_{m+1,n-1}+c_{m-1,n+1}-c_{m-1,n-1}\Big].\end{aligned} \quad (53)$$

4.3. Resonance condition and periodic approximation

Suppose now that there is a resonance of the form

$$\Delta Mc^2 \;=\; \hbar\omega_0\Delta n \quad (54)$$

(since $\Delta\omega(E)$ is zero in the resonant sector) with Δn odd. In this case, the eigenvalue equation becomes locally approximately periodic; in this case we require [19]

$$\left(\mathbf{a}\cdot c\frac{\mathrm{d}\mathbf{P}}{\mathrm{d}a}\right)\sqrt{n}\sqrt{S^2-m^2} \tag{55}$$

and

$$\frac{n}{2}\hbar\Delta\omega(E) \tag{56}$$

to be approximately constant locally for indirect transitions of the form

$$(n+\Delta n, m-1) \;\rightarrow\; (n,m) \;\rightarrow\; (n-\Delta n, m+1). \tag{57}$$

In this case, we can make use of an approximate local solution of the form

$$c_{m,n} \;\rightarrow\; \mathrm{e}^{im\phi}v_{n+m\Delta n}, \tag{58}$$

which is consistent with an approximate local wavefunction of the form

$$\Psi \;=\; \sum_m\sum_n \mathrm{e}^{im\phi}v_{n+m\Delta n}|n\rangle|S,m\rangle. \tag{59}$$

The eigenvalue equation for the v coefficients in this local approximation satisfy

$$\begin{aligned}E(\phi)v_n \;=\; &\left\{\hbar\left[\omega_0+\Delta\omega(E)\right]n - i\frac{\hbar}{2}\Gamma(E)\right\}v_n - \frac{n}{2}\hbar\Delta\omega(E)\left[v_{n+2}+v_{n-2}\right]\\ &+\left(\mathbf{a}\cdot c\frac{\mathrm{d}\mathbf{P}}{\mathrm{d}a}\right)\sqrt{n}\sqrt{S^2-m^2}\left[\mathrm{e}^{i\phi}\left(v_{n+\Delta n+1}+v_{n+\Delta n-1}\right)+\mathrm{e}^{-i\phi}\left(v_{n-\Delta n+1}+v_{n-\Delta n-1}\right)\right].\end{aligned} \tag{60}$$

Although we have used the notation $E(\phi)$ for the energy eigenvalue here, if we wish to relate it to the energy eigenvalue E above we will need to remember that a constant offset of ΔMc^2m has been suppressed.

4.4. Implementing loss as a boundary condition

There seems to be nothing to prevent us from making use of a realistic loss model for $\hat{\Gamma}(E)$ in this approximation, and computing the sector eigenfunctions and eigenvalues in the Brillouin-Wigner formalism that we are using. However, we know that when the loss is very large for basis states with an energy below the resonant sector energy $E(\phi)$, that the state occupation will be very small. We implement this boundary condition approximately by omitting basis states with n less than n_0. We therefore consider the local eigenvalue equation

$$\begin{aligned}E(\phi)v_n \;=\; &\hbar\left[\omega_0+\Delta\omega(E)\right]nv_n - \frac{n}{2}\hbar\Delta\omega(E)\left[v_{n+2}+v_{n-2}\right]\\ &+\left(\mathbf{a}\cdot c\frac{\mathrm{d}\mathbf{P}}{\mathrm{d}a}\right)\sqrt{n}\sqrt{S^2-m^2}\left[\mathrm{e}^{i\phi}\left(v_{n+\Delta n+1}+v_{n+\Delta n-1}\right)+\mathrm{e}^{-i\phi}\left(v_{n-\Delta n+1}+v_{n-\Delta n-1}\right)\right]\end{aligned} \tag{61}$$

with

$$v_n \;\rightarrow\; 0 \qquad \text{for } n \;\leq\; n_0 \tag{62}$$

This version of the local approximation eigenvalue equation is a bit different than previous versions [19,20]. Here we are interested in taking into account the $\sqrt{n}$ dependence of the coupling strength in the second line, so that n in this version of the model will be the number of phonons (instead of an incremental number of phonons).

4.5. Approximate model for the nuclear state distribution

Historically our focus has been on the phonon distribution, since the solution of the local problem determines the indirect matrix element (from which the rate of coherent energy transfer is determined). However, it has become clear that if we have an approximate solution for the v_n coefficients, these could be used to develop a consistent model for which m states are occupied. Such a model could be quite useful to determine the m distribution near the threshold for coherent dynamics.

For this we propose an approximate product solution of the form

$$c_{m,n} \;=\; (-1)^m d_m v_{n+m\Delta n}. \tag{63}$$

We propose to find a constraint on the d_m by using the variational principle on an approximate total energy. For this we start with

$$\begin{aligned}
\langle \hat{H} \rangle \;=\; & \sum_{m,n} \left\{ \Delta M c^2 m + \hbar \left[\omega_0 + \Delta\omega(E) \right] \left(n + \frac{1}{2} \right) \right\} |c_{m,n}|^2 \\
& + \sum_{m,n} \left(\mathbf{a} \cdot c \frac{\mathrm{d}\mathbf{P}}{\mathrm{d}a} \right) \sqrt{(S-m)(S+m+1)} \left[\sqrt{n+1} c_{m,n} c_{m+1,n+1} + \sqrt{n} c_{m,n} c_{m+1,n-1} \right] \\
& + \sum_{m,n} \left(\mathbf{a} \cdot c \frac{\mathrm{d}\mathbf{P}}{\mathrm{d}a} \right) \sqrt{(S+m)(S-m+1)} \left[\sqrt{n+1} c_{m,n} c_{m-1,n+1} + \sqrt{n} c_{m,n} c_{m-1,n-1} \right] \\
& - \sum_{m,n} \frac{1}{2} \hbar \Delta\omega(E) \left[\sqrt{(n+2)(n+1)} c_{m,n} c_{m,n+2} + \sqrt{n(n-1)} c_{m,n} c_{m,n-2} \right],
\end{aligned} \tag{64}$$

where the summations are over allowed states. This we adapt to a product approximation using

$$\begin{aligned}
\langle \hat{H} \rangle \;=\; & \sum_{m,n} \left\{ \Delta M c^2 m + \hbar \left[\omega_0 + \Delta\omega(E) \right] \left(n + \frac{1}{2} \right) \right\} |d_m|^2 v_n^2 \\
& - \left(\mathbf{a} \cdot c \frac{\mathrm{d}\mathbf{P}}{\mathrm{d}a} \right) \left[\sum_n \sqrt{n+1} v_n v_{n+1} + \sqrt{n} v_n v_{n-1} \right] \\
& \left[\sum_m \sqrt{(S-m)(S+m+1)} d_m d_{m+1} + \sqrt{(S+m)(S-m+1)} d_m d_{m-1} \right] \\
& - \sum_{m,n} \frac{1}{2} \hbar \Delta\omega(E) |d_m|^2 \left[\sqrt{(n+2)(n+1)} v_n v_{n+2} + \sqrt{n(n-1)} v_n v_{n-2} \right].
\end{aligned} \tag{65}$$

Minimization of the energy with respect to the d_m coefficients results in

$$\begin{aligned} E_d d_m \;=\; & \sum_n \left\{ \Delta M c^2 m + \hbar \left[\omega_0 + \Delta\omega(E) \right] \left(n + \frac{1}{2} \right) \right\} v_n^2 d_m \\ & - \left(\mathbf{a} \cdot c \frac{\mathrm{d}\mathbf{P}}{\mathrm{d}a} \right) \left[\sum_n \sqrt{n+1} v_n v_{n+1} + \sqrt{n} v_n v_{n-1} \right] \\ & \left[\sqrt{(S-m)(S+m+1)} d_{m+1} + \sqrt{(S+m)(S-m+1)} d_{m-1} \right] \\ & - \sum_n \frac{1}{2} \hbar \Delta\omega(E) \left[\sqrt{(n+2)(n+1)} v_n v_{n+2} + \sqrt{n(n-1)} v_n v_{n-2} \right] d_m . \end{aligned} \tag{66}$$

This provides an improved constraint over one proposed previously in [38].

4.6. Reduction of the constraint

We would like to isolate terms in this eigenvalue equation that depend on m. For example, consider

$$\sum_n \left\{ \hbar \left[\omega_0 + \Delta\omega(E) \right] \left(n + \frac{1}{2} \right) \right\} v_n^2 \;\rightarrow\; \hbar\omega_0 \left(\langle n \rangle + \frac{1}{2} \right) + \hbar \langle n \Delta\omega \rangle + \frac{1}{2} \hbar \langle \Delta\omega \rangle . \tag{67}$$

This term has no m dependence, and only provides a constant offset. Our constraint is then equivalent to

$$E'_d d_m \;=\; \Delta M c^2 m d_m - 2 \left(\mathbf{a} \cdot c \frac{\mathrm{d}\mathbf{P}}{\mathrm{d}a} \right) \langle \sqrt{n} \rangle \left[\sqrt{(S-m)(S+m+1)} d_{m+1} + \sqrt{(S+m)(S-m+1)} d_{m-1} \right], \tag{68}$$

which we can write in normalized form as

$$\lambda_d d_m \;=\; m d_m - 2 \frac{\left(\mathbf{a} \cdot c \frac{\mathrm{d}\mathbf{P}}{\mathrm{d}a} \right) \langle \sqrt{n} \rangle}{\Delta M c^2} \left[\sqrt{(S-m)(S+m+1)} d_{m+1} + \sqrt{(S+m)(S-m+1)} d_{m-1} \right]. \tag{69}$$

4.7. Specialization for threshold calculations

In the case of lattice-induced nuclear excitation, the population of the nuclei to be excited is localized near the ground state. In previous work we pursued models specific to this limit; to proceed, we recall the relation between the Dicke parameters S and m and the number of nuclei in the two states

$$S - m \;=\; N_0 - N_1, \qquad S + m \;=\; N_1, \tag{70}$$

where N_0 is the total number of nuclei, and where N_1 is the number of excited state nuclei. We will assume that the number of nuclei in each state is much greater than unity

$$N_0 - N_1 \;\gg\; 1, \qquad N_1 \;\gg\; 1 \tag{71}$$

in which case the Dicke factors reduce to

$$\sqrt{(S-m)(S+m+1)} \;\rightarrow\; \sqrt{(N_0-N_1)N_1}, \tag{72}$$

$$\sqrt{(S+m)(S-m+1)} \;\rightarrow\; \sqrt{N_1(N_0-N_1)}. \tag{73}$$

The eigenvalue equation can be written in terms of the number of excited nuclei as

$$\lambda'_d d_{N_1} \;=\; N_1 d_{N_1} - 2\frac{\left(\mathbf{a}\cdot c\frac{\mathrm{d}\mathbf{P}}{\mathrm{d}a}\right)\langle\sqrt{n}\rangle\sqrt{(N_0-N_1)N_1}}{\Delta M c^2}\Big(d_{N_1+1}+d_{N_1-1}\Big). \tag{74}$$

We can make use of this constraint to estimate state distributions for the computation of average quantities that show up later on. This version of the constraint is most closely related to those of [38] (note that a factor of N_1 is missing in the potential of Eqs. (57) and (58) and several following equations in [38]).

Although we have considered a similar constraint in our earlier work, this new version of the constraint works very differently. We will see an enhancement in the fractionation power resulting from this constraint.

5. Pulse and Amplitude Approximation

Since the solutions to the local eigenvalue equation includes a series of pulses that are very nearly the same, we have found it effective to make use of a pulse and amplitude approximation [20,39]. Adapting the pulse and amplitude approximation to the present case we may write for the $\phi = \pi$ case

$$v_n^{(-)} \;\rightarrow\; \sum_{j=0}^{\infty}\sum_{k=0}^{\Delta n-1} \delta_{j\Delta n+k-n}\, a_j u_k, \tag{75}$$

For the other case ($\phi = 0$) we have

$$(-1)^n v_n^{(+)} \;\rightarrow\; \sum_{j=0}^{\infty}\sum_{k=0}^{\Delta n-1} \delta_{j\Delta n+k-n}\, a_j u_k. \tag{76}$$

5.1. Total energy

To optimize the pulse and amplitude solutions individually, we would like to use an appropriate variational method based on the total energy. We start with the total pulse energy in terms of the v_n, which is

$$\begin{aligned}\langle v_n|\hat{H}|v_n\rangle \;=\; & \sum_n \hbar\Big[\omega_0+\Delta\omega_n\Big]n v_n^2 - \sum_n \frac{n}{2}\hbar\Delta\omega_n v_n\Big[v_{n+2}+v_{n-2}\Big] \\ & \pm\left(\mathbf{a}\cdot c\frac{d\mathbf{P}}{da}\right)\sqrt{S^2-m^2}\sum_n \sqrt{n}\, v_n\Big[v_{n+\Delta n+1}+v_{n+\Delta n-1}+v_{n-\Delta n+1}+v_{n-\Delta n-1}\Big].\end{aligned} \tag{77}$$

In the pulse and amplitude approximation we adapt this to

$$\begin{aligned}\langle v_n|\hat{H}|v_n\rangle \;=\; & \sum_j \sum_k \hbar\Big[\omega_0 + \Delta\omega_{j\Delta n+k}\Big](j\Delta n+k)a_j^2 u_k^2 \\ & - \sum_j \sum_k \frac{j\Delta n+k}{2}\hbar\Delta\omega_{j\Delta n+k}a_j^2 u_k\Big[u_{k+2}+u_{k-2}\Big] \\ & - \left(\mathbf{a}\cdot c\frac{\mathrm{d}\mathbf{P}}{\mathrm{d}a}\right)\sqrt{S^2-m^2}\sum_j\sum_k\sqrt{j\Delta n+k}\Big[a_j a_{j+1}+a_j a_{j-1}\Big]\Big[u_k u_{k+1}+u_k u_{k-1}\Big]. \end{aligned} \tag{78}$$

5.2. Optimization of the amplitudes

We begin with the optimization of the amplitudes, which is accomplished by minimizing the energy to give the constraint

$$\begin{aligned} E_a a_j \;=\; & \left\{\sum_k \hbar\Big[\omega_0+\Delta\omega_{j\Delta n+k}\Big](j\Delta n+k)u_k^2 - \sum_k \frac{j\Delta n+k}{2}\hbar\Delta\omega_{j\Delta n+k}u_k\Big[u_{k+2}+u_{k-2}\Big]\right\}a_j \\ & - \left(\mathbf{a}\cdot c\frac{\mathrm{d}\mathbf{P}}{\mathrm{d}a}\right)\sqrt{S^2-m^2}\left\{\sum_k\sqrt{j\Delta n+k}\Big[u_k u_{k+1}+u_k u_{k-1}\Big]\right\}\Big(a_{j+1}+a_{j-1}\Big). \end{aligned} \tag{79}$$

In general we are interested in this model under conditions where

$$j \;\gg\; 1 \tag{80}$$

so that

$$\sum_k \hbar\Big[\omega_0+\Delta\omega_{j\Delta n+k}\Big](j\Delta n+k)u_k^2 \;\to\; j\hbar\Big[\omega_0+\Delta\omega_{j\Delta n}\Big]\Delta n, \tag{81}$$

$$\sum_k \frac{j\Delta n+k}{2}\hbar\Delta\omega_{j\Delta n+k}u_k\Big[u_{k+2}+u_{k-2}\Big] \;\to\; j\Delta n\hbar\Delta\omega_{j\Delta n}, \tag{82}$$

$$\sum_k \sqrt{j\Delta n+k}\Big[u_k u_{k+1}+u_k u_{k-1}\Big] \;\to\; 2\sqrt{j}\sqrt{\Delta n}. \tag{83}$$

This leads to

$$E_a a_j \;=\; j\Delta M c^2 a_j - \left\{2\left(\mathbf{a}\cdot c\frac{\mathrm{d}\mathbf{P}}{\mathrm{d}a}\right)\sqrt{\Delta n}\sqrt{S^2-m^2}\right\}\sqrt{j}\Big(a_{j+1}+a_{j-1}\Big). \tag{84}$$

It would seem reasonable to normalize this equation, and also modify it into the form

$$\lambda_a a_j \;=\; j a_j - 2\frac{\left(\mathbf{a}\cdot c\frac{\mathrm{d}\mathbf{P}}{\mathrm{d}a}\right)\sqrt{\Delta n}\sqrt{S^2-m^2}}{\Delta M c^2}\left(\sqrt{j+1}\,a_{j+1}+\sqrt{j}\,a_{j-1}\right), \tag{85}$$

where

$$\lambda_a \;=\; \frac{E_a}{\Delta M c^2} \tag{86}$$

Note that this model generalizes the result obtained previously in [39].

Once again, it seems worth emphasizing that this version of the amplitude constraint differs in an important way from what we considered previously; this one includes the enhancement of the coupling when the number of phonons increase.

5.3. Pulse optimization

We next optimize the pulse by minimizing the energy to obtain the constraint

$$\begin{aligned} E_u u_k \;=\; & \left\{\sum_j \hbar\Big[\omega_0+\Delta\omega_{j\Delta n+k}\Big](j\Delta n+k)a_j^2\right\}u_k \\ & -\left\{\sum_j \frac{j\Delta n+k}{2}\hbar\Delta\omega_{j\Delta n+k}a_j^2\right\}\Big(u_{k+2}+u_{k-2}\Big) \\ & -\left\{\left(\mathbf{a}\cdot c\frac{\mathrm{d}\mathbf{P}}{\mathrm{d}a}\right)\sqrt{S^2-m^2}\sum_j\sqrt{j\Delta n+k}\,\Big[a_j a_{j+1}+a_j a_{j-1}\Big]\right\}\Big(u_{k+1}+u_{k-1}\Big), \end{aligned} \tag{87}$$

Once again we assume that j is large, and approximate

$$\sum_j \hbar\Big[\omega_0+\Delta\omega_{j\Delta n+k}\Big](j\Delta n+k)a_j^2 \;\to\; \Delta n\hbar\Big[\omega_0\langle j\rangle+\langle j\Delta\omega\rangle\Big]+\hbar\Big[\omega_0+\langle\Delta\omega\rangle\Big]k, \tag{88}$$

$$\sum_j \frac{j\Delta n+k}{2}\hbar\Delta\omega_{j\Delta n+k}a_j^2 \;\to\; \frac{1}{2}\Delta n\hbar\langle j\Delta\omega\rangle+\frac{1}{2}\Delta n\hbar\langle\Delta\omega\rangle k, \tag{89}$$

$$\sum_j \sqrt{j\Delta n+k}\,\Big[a_j a_{j+1}+a_j a_{j-1}\Big] \;\to\; 2\sqrt{\Delta n}\langle\sqrt{j}\rangle. \tag{90}$$

The pulse equation that results can be written as

$$\left[E_u - \Delta n\hbar\Big(\omega_0\langle j\rangle + \langle j\Delta\omega\rangle\Big)\right]u_k \;=\; \hbar\Big[\omega_0 + \langle\Delta\omega\rangle\Big]ku_k - \left\{\frac{1}{2}\Delta n\hbar\langle j\Delta\omega\rangle + \frac{1}{2}\Delta n\hbar\langle\Delta\omega\rangle k\right\}\Big(u_{k+2} + u_{k-2}\Big) - 2\left\{\left(\mathbf{a}\cdot c\frac{\mathrm{d}\mathbf{P}}{\mathrm{d}a}\right)\sqrt{S^2-m^2}\sqrt{\Delta n}\langle\sqrt{j}\rangle\right\}\Big(u_{k+1} + u_{k-1}\Big). \tag{91}$$

We would like to take advantage of the fact that

$$k \;\ll\; j\Delta n \tag{92}$$

in this constraint. To do this, we will use the approximation

$$\hbar\Big[\omega_0 + \langle\Delta\omega\rangle\Big]ku_k - \left\{\frac{1}{2}\Delta n\hbar\langle j\Delta\omega\rangle + \frac{1}{2}\Delta n\hbar\langle\Delta\omega\rangle k\right\}\Big(u_{k+2} + u_{k-2}\Big) \;\rightarrow\; \hbar\omega_0 ku_k - \frac{1}{2}\Delta n\hbar\langle j\Delta\omega\rangle\Big(u_{k+2} + u_{k-2}\Big). \tag{93}$$

The approximate pulse constraint that results can be written as

$$E'_u u_k \;=\; \hbar\omega_0 ku_k - \frac{1}{2}\Delta n\hbar\langle j\Delta\omega\rangle\Big(u_{k+2} + u_{k-2}\Big) - 2\left\{\left(\mathbf{a}\cdot c\frac{\mathrm{d}\mathbf{P}}{\mathrm{d}a}\right)\sqrt{S^2-m^2}\sqrt{\Delta n}\langle\sqrt{j}\rangle\right\}\Big(u_{k+1} + u_{k-1}\Big). \tag{94}$$

As before it seems useful to have a normalized version of this constraint, which we can write as

$$\lambda_u u_k \;=\; ku_k - \frac{\Delta n}{2}\frac{\langle j\Delta\omega\rangle}{\omega_0}\Big(u_{k+2} + u_{k-2}\Big) - 2\left[\frac{\left(\mathbf{a}\cdot c\frac{\mathrm{d}\mathbf{P}}{\mathrm{d}a}\right)\sqrt{S^2-m^2}\sqrt{\Delta n}\langle\sqrt{j}\rangle}{\hbar\omega_0}\right]\Big(u_{k+1} + u_{k-1}\Big). \tag{95}$$

This is similar to what we obtained previously in Ref. [39], but is generalized to include the effects of phonon fluctuations. Since we have analyzed this kind of problem previously, our attention is drawn here to the prefactors of the fluctuation terms (those containing $u_{k'}$ with $k' \neq k$), as these determine the indirect coupling matrix element which determines the coherent energy exchange rate [20].

6. Estimation of the Indirect Coupling Matrix Element

We are interested in developing estimates for the coherent energy exchange rate under conditions of fractionation. This rate is proportional to the indirect coupling matrix element, and from previous work we know that the pulse and amplitude approximation can be used to obtain accurate estimates for the indirect coupling matrix element. As we have seen above, there are three constraints that describe the different distributions of states that are relevant to the problem (pulse, amplitude and nuclear excited state distribution). In this section we will examine these constraints, and use them to estimate the indirect coupling matrix element.

6.1. Amplitude constraint

We will work with the amplitude constraint in the form

$$\lambda_a a_j \;=\; j a_j - 2\gamma_a \left(\sqrt{j+1}\, a_{j+1} + \sqrt{j}\, a_{j-1} \right) \tag{96}$$

with

$$\gamma_a \;=\; \frac{\left(\mathbf{a} \cdot c \dfrac{\mathrm{d}\,\mathbf{P}}{\mathrm{d}a} \right) \sqrt{\Delta n} \sqrt{S^2 - m^2}}{\Delta M c^2} \tag{97}$$

subject to the boundary condition

$$a_j \;=\; 0 \qquad \text{for } j \;<\; j_0, \tag{98}$$

where

$$j_0 \;=\; \frac{n_0}{\Delta n}. \tag{99}$$

We have discussed this kind of problem previously [20,39], so we know how it works and how to use it. We are not interested in the eigenvalue; however, we are very interested in the expansion coefficients a_j because they can be used to determine expectation values needed for the model.

6.2. Scaling relations

There is no difficulty solving this eigenvalue equation numerically, which is of interest here to develop scaling laws for the expectation values that we need for the pulse constraint. From the numerical solutions we can estimate

$$\langle \sqrt{j} \rangle \;\rightarrow\; \sqrt{j_0 + (2\gamma_a)^2}. \tag{100}$$

We also require the expectation value of the frequency shift

$$\begin{aligned} \langle \Delta\omega \rangle \;&=\; \left[\frac{\mathrm{d}}{\mathrm{d}E} \Delta\omega \right] \frac{\Delta M c^2}{j \Delta n} (j \Delta n - n_0) \\ &=\; \left[\frac{\mathrm{d}}{\mathrm{d}E} \Delta\omega \right] \hbar\omega_0 \left\langle \frac{j - j_0}{j} \right\rangle . \end{aligned} \tag{101}$$

There are three regimes of interest; we may write

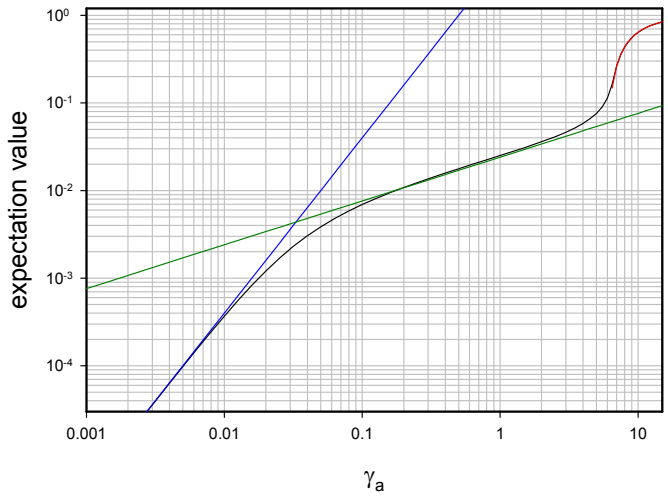

Figure 1. Numerical (black) and analytic (blue, green, and red) results for $\langle (j - j_0)/j \rangle$ as a function of γ_a, for $j_0 = 144$.

$$\left\langle \frac{j - j_0}{j} \right\rangle = \begin{cases} 4\gamma_a^2, & \gamma_a < \dfrac{1}{4^{2/3}\sqrt{j_0}}, \\ \dfrac{\sqrt{\gamma_a}}{j_0^{3/4}}, & \dfrac{1}{4^{2/3}\sqrt{j_0}} < \gamma_a < \dfrac{\sqrt{j_0}}{2}, \\ 1 - \dfrac{j_0}{4\gamma_a^2}, & \gamma_a > \dfrac{\sqrt{j_0}}{2}. \end{cases} \tag{102}$$

The different limits are compared with exact numerical results in Fig. 1. Finally, we require

$$\langle j \Delta\omega \rangle = \left[\frac{\mathrm{d}}{\mathrm{d}E} \Delta\omega \right] \hbar\omega_0 \langle j - j_0 \rangle \tag{103}$$

Once again there are three regimes of interest; we have the estimates

$$\langle j - j_0 \rangle = \begin{cases} 4\gamma_a^2 j_0, & \gamma_a < \dfrac{1}{4^{2/3}\sqrt{j_0}}, \\ j_0^{1/4}\sqrt{\gamma_a}, & \dfrac{1}{4^{2/3}\sqrt{j_0}} < \gamma_a < \dfrac{\sqrt{j_0}}{2}, \\ 4\gamma_a^2 - j_0, & \gamma_a > \dfrac{\sqrt{j_0}}{2}. \end{cases} \tag{104}$$

Once we have the scaling relations for the expectation values, we have everything with need from the amplitude constraint.

6.3. Pulse constraint

We can write the pulse constraint as

$$\lambda_u u_k \;=\; k u_k - \frac{g'_u}{2}\Big(u_{k+2}+u_{k-2}\Big) - 2g_u\Big(u_{k+1}+u_{k-1}\Big) \tag{105}$$

with

$$\begin{aligned} g_u \;&=\; \frac{\left(\mathbf{a}\cdot c\dfrac{\mathrm{d}\mathbf{P}}{\mathrm{d}a}\right)\sqrt{S^2-m^2}\sqrt{\Delta n}\langle\sqrt{j}\rangle}{\hbar\omega_0} \\ &=\; \gamma_a \Delta n \langle\sqrt{j}\rangle, \end{aligned} \tag{106}$$

$$g'_u \;=\; \Delta n \frac{\langle j\,\Delta\omega\rangle}{\omega_0}. \tag{107}$$

Once again, we have encountered this kind of constraint previously [20,39], and we know that the indirect coupling matrix element can be derived from the g_u and g'_u parameters.

Since we are interested in situations where Δn is very large, and since we know that the u_n vary slowly when the coupling is strong, we can develop a continuum version of the constraint according to

$$\lambda_u u(z) \;=\; \Delta n z u(z) - \frac{g'_u}{2}\left[2u(z)+\frac{4}{\Delta n^2}\frac{\mathrm{d}^2}{\mathrm{d}z^2}u(z)\right] - 2g_u\left[2u(z)+\frac{1}{\Delta n^2}\frac{\mathrm{d}^2}{\mathrm{d}z^2}u(z)\right]. \tag{108}$$

This can be simplified to

$$\epsilon u(z) \;=\; z u(z) - \frac{2(g_u+g'_u)}{(\Delta n)^3}\frac{\mathrm{d}^2}{\mathrm{d}z^2}u(z). \tag{109}$$

6.4. Impact of fluctuations

We are interested in understanding under what conditions fluctuation might be important. To study this, we examine the ratio of the two dimensionless coupling constants

$$\frac{g'_u}{g_u} \;\to\; \hbar\left[\frac{\mathrm{d}}{\mathrm{d}E}\Delta\omega\right]\begin{cases} \gamma_a\sqrt{j_0}, & \gamma_a\sqrt{j_0} \;<\; \dfrac{1}{4^{2/3}}, \\[2ex] \dfrac{1}{\sqrt{j_0}\gamma_a}, & \dfrac{1}{4^{2/3}\sqrt{j_0}} \;<\; \gamma_a \;<\; \dfrac{\sqrt{j_0}}{2}, \\[2ex] 2, & \gamma_a \;>\; \dfrac{\sqrt{j_0}}{2}. \end{cases} \tag{110}$$

Earlier we obtained an estimate for the frequency shift for Na in the Bloch picture, which we write here as

$$\hbar \left[\frac{\mathrm{d}}{\mathrm{d}E} \Delta\omega \right] \; = \; 0.013. \tag{111}$$

We see that fluctuations will have the largest impact in the outer two regions generally, and for Na in the Bloch model in particular we can write

$$\frac{g'_u}{g_u} \; \rightarrow \; \begin{cases} 0.013 \gamma_a \sqrt{j_0}, & \gamma_a \sqrt{j_0} \; < \; \dfrac{1}{4^{2/3}}, \\ \dfrac{0.013}{\sqrt{j_0 \gamma_a}}, & \dfrac{1}{4^{2/3}\sqrt{j_0}} \; < \; \gamma_a \; < \; \dfrac{\sqrt{j_0}}{2}, \\ 0.026, & \gamma_a \; > \; \dfrac{\sqrt{j_0}}{2}. \end{cases} \tag{112}$$

In general, fluctuations contribute only a minor correction in the Bloch picture. The fluctuations can be larger in the Born–Oppenheimer approximation where appropriate, which suggests that we should think about them further in connection with experiments involving nanoparticles.

6.5. Indirect coupling matrix element

We can write for the indirect coupling matrix element [20]

$$\frac{V_{\mathrm{eff}}}{\Delta M c^2} \; = \; 4 \frac{2(g_u + g'_u)}{(\Delta n)^3} \; \Phi \left[\frac{2(g_u + g'_u)}{(\Delta n)^3} \right], \tag{113}$$

where the Φ function was defined previously in connection with the lossy spin–boson problem [20], and illustrated in Fig. 2.

The coherent energy exchange rate is proportional to this indirect coupling matrix element [20]. From earlier work we view the indirect coupling matrix element as involving a prefactor which is sufficiently large as to allow for very fast reactions as long as the large quantum can be fractionated; and a hindrance factor, which in this case is the Φ function, which approaches unity only when the associated coupling is sufficiently strong. The hindrance factor here is then associated with the fractionation of the quantum, which is the most difficult thing accomplished by the model.

7. Threshold Condition for Lattice-induced Nuclear Excitation

From the beginning of the field back in 1989, the key issue in our view has always been whether a large quantum can be fractionated. Based on the analysis in the previous sections, and also in previous papers, we are in a position to evaluate the threshold condition for fractionation. The basic argument is that the coupling has to be sufficiently strong in order for a large quantum to be fractionated, and now we can quantify this.

7.1. Threshold condition

The Φ function that shows up in the evaluation of the indirect coupling matrix element is essentially a hindrance factor, one that goes approximately to unity when the coupling is strong

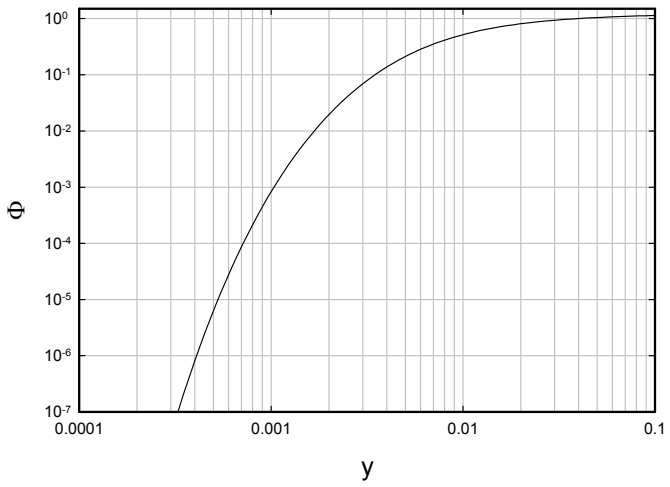

Figure 2. Function $\Phi(y)$ as a function of y.

$$\lim_{x>0.03} \Phi(x) \;\rightarrow\; 1. \tag{114}$$

Alternatively, when the coupling is weak, the hindrance function Φ goes to zero. We will adopt a threshold condition here based on

$$\frac{2(g_u + g'_u)}{(\Delta n)^3} \;\geq\; 4 \times 10^{-4}. \tag{115}$$

In the event that can neglect fluctuations, this becomes

$$\frac{2g_u}{(\Delta n)^3} \;=\; \frac{2\gamma_a \langle\sqrt{j}\rangle}{(\Delta n)^2} \;\geq\; 4 \times 10^{-4}. \tag{116}$$

This then is the mathematical requirement that needs to be satisfied for the large quantum ΔMc^2 to be fractionated into Δn smaller quanta $\hbar\omega_0$. In what follows our goal is to relate this mathematical constraint to the relevant parameters of a physical system.

7.2. Expectation value of the Dicke number

If we expand out this constraint, we obtain

$$\frac{2\left(\mathbf{a}\cdot c\frac{\mathrm{d}\mathbf{P}}{\mathrm{d}a}\right)\sqrt{\Delta n}\sqrt{S^2-m^2}\langle\sqrt{j}\rangle}{\Delta Mc^2(\Delta n)^2} \;\geq\; 4\times 10^{-4}. \tag{117}$$

Before proceeding, we require an estimate for the Dicke factor $\sqrt{S^2-m^2}$. We recall that

$$\sqrt{S^2-m^2} \;=\; \sqrt{(N_0-N_1)N_1}. \tag{118}$$

The total rate will be obtained by averaging the N_1-dependent rate over the relevant distribution; however, for the simple argument in this section, we will be satisfied with an average.

To proceed, we need to determine the population distribution from the eigenvalue equation that we derived previously

$$\lambda'_d d_{N_1} \;=\; N_1 d_{N_1} - 2\frac{\left(\mathbf{a}\cdot c\frac{\mathrm{d}\mathbf{P}}{\mathrm{d}a}\right)\langle\sqrt{n}\rangle\sqrt{(N_0-N_1)N_1}}{\Delta Mc^2}\left(d_{N_1+1}+d_{N_1-1}\right). \tag{119}$$

At issue here is the fact that $\langle\sqrt{n}\rangle$ depends on N_1

$$\begin{aligned}\langle\sqrt{n}\rangle \;&\rightarrow\; \sqrt{\Delta n}\langle\sqrt{j}\rangle \;\rightarrow\; \sqrt{\Delta n}\sqrt{j_0+4\gamma_a^2} \\ &= \sqrt{n_0}\sqrt{1+\frac{4\left(\mathbf{a}\cdot c\frac{\mathrm{d}\mathbf{P}}{\mathrm{d}a}\right)^2\Delta n(N_0-N_1)N_1}{j_0(\Delta Mc^2)^2}}.\end{aligned} \tag{120}$$

It will be useful to write this as

$$\sqrt{n} \;\rightarrow\; \sqrt{n_0}\sqrt{1+\frac{(N_0-N_1)N_1}{N_0N_c}}, \tag{121}$$

where

$$N_c \;=\; \frac{j_0(\Delta Mc^2)^2}{4\left(\mathbf{a}\cdot c\frac{\mathrm{d}\mathbf{P}}{\mathrm{d}a}\right)^2\Delta nN_0} \;=\; \frac{n_0(\hbar\omega_0)^2}{4\left(\mathbf{a}\cdot c\frac{\mathrm{d}\mathbf{P}}{\mathrm{d}a}\right)^2N_0}. \tag{122}$$

The eigenvalue equation for the d_{N_1} then becomes

$$\lambda'_d d_{N_1} \;=\; N_1 d_{N_1} - 2\gamma_d\sqrt{\frac{(N_0-N_1)N_1}{N_0}}\sqrt{1+\frac{(N_0-N_1)N_1}{N_0N_c}}\left(d_{N_1+1}+d_{N_1-1}\right), \tag{123}$$

where

$$\gamma_d \;=\; \frac{\left(\mathbf{a}\cdot c\frac{\mathrm{d}\,\mathbf{P}}{\mathrm{d}a}\right)\sqrt{n_0}\sqrt{N_0}}{\Delta Mc^2}. \tag{124}$$

As before in the case of the amplitude eigenvalue equation, we are not interested in the eigenvalue; however, we are interested in the expansion coefficients, since we can use them to calculate the expectation value $\left\langle\sqrt{S^2-m^2}\langle j\rangle\right\rangle$.

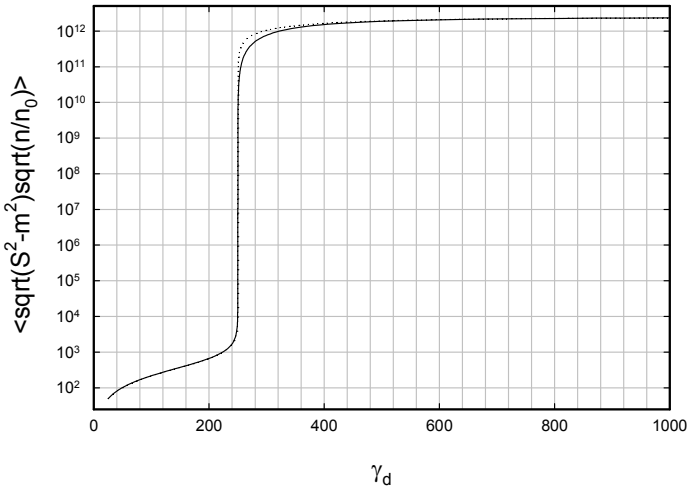

Figure 3. Numerical result for $\left\langle \sqrt{S^2-m^2}\frac{\langle\sqrt{n}\rangle}{\sqrt{n_0}}\right\rangle$ as a function of γ_d (solid line) compared with empirical result of Eq. (125); in this calculation we have taken $N_0 = 10^{16}$ and $N_c = 10^6$.

We have solved numerically for the excited state distribution by now many times, and we have found empirical formula for the required expectation value of the form

$$\left\langle \sqrt{S^2-m^2}\langle\sqrt{n}\rangle\right\rangle \;=\; \sqrt{\Delta n}\left\langle \sqrt{S^2-m^2}\langle\sqrt{j}\rangle\right\rangle$$

$$\rightarrow \begin{cases} \sqrt{n_0 N_0}\dfrac{2\gamma_d}{\sqrt{1-\left(\dfrac{4\gamma_d}{\sqrt{N_c}}\right)^2}}, & 4\gamma_d < \sqrt{N_c}, \\ \dfrac{1}{4}\sqrt{n_0 N_0}\dfrac{N_0}{\sqrt{N_c}}\sqrt{\dfrac{1-\left(\dfrac{\sqrt{N_c}}{4\gamma_d}\right)^2}{1+\left(\dfrac{\sqrt{N_c}}{4\gamma_d}\right)^2}}, & 4\gamma_d > \sqrt{N_c}. \end{cases} \tag{125}$$

We have not considered this expectation value before; it is new to this analysis of the model. Note from Fig. 3 that this matrix element increases suddenly at $\gamma_d = \sqrt{N_c}/4$, which implies for us a corresponding sudden increase in the ability of the system to fractionate a large quantum.

7.3. Threshold constraint including the averaged Dicke factor

We can make use of the results above and write the constraint in the form

$$4\times 10^{-4} \;\leq\; \frac{2\left(\mathbf{a}\cdot c\frac{\mathrm{d}\mathbf{P}}{\mathrm{d}a}\right)\sqrt{n_0N_0}}{\Delta Mc^2(\Delta n)^2}\times\begin{cases}\dfrac{2\gamma_d}{\sqrt{1-\left(\dfrac{4\gamma_d}{\sqrt{N_c}}\right)^2}}, & 4\gamma_d<\sqrt{N_c},\\[2ex] \dfrac{1}{4}\dfrac{N_0}{N_c^{1/2}}\sqrt{\dfrac{1-\left(\dfrac{\sqrt{N_c}}{4\gamma_d}\right)^2}{1+\left(\dfrac{\sqrt{N_c}}{4\gamma_d}\right)^2}}, & 4\gamma_d>\sqrt{N_c}.\end{cases} \tag{126}$$

Let us first consider the case of $4\gamma_d < \sqrt{N_c}$, which we might consider to be a conventional regime (conventional in the sense that the number of virtual phonons is less than the number of real phonons, and there is no large enhancement of virtual nuclear excited state population). Away from the boundary the constraint becomes

$$\frac{2\left(\mathbf{a}\cdot c\frac{\mathrm{d}\mathbf{P}}{\mathrm{d}a}\right)\sqrt{n_0N_0}}{\Delta Mc^2(\Delta n)^2}(2\gamma_d) \;=\; \frac{4(\hbar\omega_0)^2\left(\mathbf{a}\cdot c\frac{\mathrm{d}\mathbf{P}}{\mathrm{d}a}\right)^2 n_0N_0}{(\Delta Mc^2)^4} \;\geq\; 4\times 10^{-4}, \qquad 4\gamma_d \ll \sqrt{N_c}. \tag{127}$$

Next we examine what happens when $4\gamma_d > \sqrt{N_c}$, which will will consider to be in the anomalous regime (anomalous because there are more virtual phonons than real, and a large enhancement of virtual nuclear excitation can occur). Away from the boundary we may write

$$\frac{2\left(\mathbf{a}\cdot c\frac{\mathrm{d}\mathbf{P}}{\mathrm{d}a}\right)\sqrt{n_0N_0}}{\Delta Mc^2(\Delta n)^2}\left(\frac{1}{4}\frac{N_0}{N_c^{1/2}}\right) \;=\; \frac{\hbar\omega_0\left(\mathbf{a}\cdot c\frac{\mathrm{d}\,\mathbf{P}}{\mathrm{d}a}\right)^2 N_0^2}{(\Delta Mc^2)^3} \;\geq\; 4\times 10^{-4}, \qquad 4\gamma_d \gg \sqrt{N_c}. \tag{128}$$

Note that this anomalous regime condition can be obtained from the conventional regime condition from the replacement

$$n_0 \;\rightarrow\; \frac{N_0\Delta Mc}{4\hbar\omega_0}. \tag{129}$$

In essence, there are more virtual phonons than real in the anomalous regime [to see this, note that the effects under discussion follow from the enhancements in $\langle\sqrt{n}\rangle$ of Eqs. (120) and (121)], and we can get an estimate of how many virtual phonons are present from this replacement.

7.4. Boundary between the conventional and anomalous regimes

The boundary between the conventional and anomalous regime satisfies

$$4\gamma_d \;=\; \frac{4\left(\mathbf{a}\cdot c\frac{\mathrm{d}\mathbf{P}}{\mathrm{d}a}\right)\sqrt{n_0}\sqrt{N_0}}{\Delta Mc^2} \;=\; \sqrt{N_c} \;=\; \sqrt{\frac{n_0(\hbar\omega_0)^2}{4\left(\mathbf{a}\cdot c\frac{\mathrm{d}\mathbf{P}}{\mathrm{d}a}\right)^2 N_0}}. \tag{130}$$

We can recast this as

$$8\left(\mathbf{a}\cdot c\frac{\mathrm{d}\mathbf{P}}{\mathrm{d}a}\right)^2 N_0 \;=\; \hbar\omega_0\Delta Mc^2. \tag{131}$$

In the case of a simple monatomic crystal, we may write for $\mathrm{d}\mathbf{P}/\mathrm{d}a$ in the special case of the highly excited uniform vibrational mode

$$\frac{\mathrm{d}\mathbf{P}}{\mathrm{d}a} \;=\; \mathbf{u}\sqrt{\frac{M\hbar\omega_0}{2N}}. \tag{132}$$

In this case the boundary is determined from

$$4\,(\mathbf{a}\cdot\mathbf{u})^2\,\frac{N_0}{N} \;=\; \frac{\Delta Mc^2}{Mc^2}. \tag{133}$$

This is very interesting for a number of reasons. We interpret this as a constraint on the strength of the transition as determined by the associated matrix element. In the event that the transition matrix element and vibrational mode are aligned (so that $\mathbf{u}\cdot\mathbf{a} = |\mathbf{a}|$) then we can determine a condition for the anomalous regime as

$$|\mathbf{a}| \;\geq\; \sqrt{\frac{1}{4}\frac{N}{N_0}\frac{\Delta Mc^2}{Mc^2}} \qquad \text{(anomalous regime)}. \tag{134}$$

In the case of a transition showing coherent dynamics, we require in addition that the transition must be stable on a relevant time scale. A static transition that satisfies the constraint may be able fractionate a large quantum for a dynamic transition (for example, in a donor and receiver scheme [40]) even if it has fast loss.

7.5. Conventional regime threshold energy

Since the basic issue in this discussion is the ability of the system to fractionate a large quantum, we would like to interpret the threshold constraint in terms of how large a quantum can be fractionated. For example, in the conventional regime we can rewrite the constraint as

$$\delta E^4 \;=\; \frac{4(\hbar\omega_0)^2\left(\mathbf{a}\cdot c\frac{\mathrm{d}\mathbf{P}}{\mathrm{d}a}\right)^2 n_0 N_0}{4\times 10^{-4}} \;\geq\; (\Delta Mc^2)^4, \tag{135}$$

where

$$\delta E \;=\; 10(\hbar\omega_0)^{1/2}\left(\mathbf{a}\cdot c\frac{\mathrm{d}\mathbf{P}}{\mathrm{d}a}\right)^{1/2}(n_0N_0)^{1/4}. \tag{136}$$

In the case of a monatomic crystal this becomes (assuming the transition is aligned with the vibrations)

$$\delta E \;=\; 8.41\;(Mc^2)^{1/4}|\mathbf{a}|^{1/2}(\hbar\omega_0)^{1/2}\left(\frac{n_0\hbar\omega_0}{N}\right)^{1/4}N_0^{1/4}. \tag{137}$$

Although an evaluation of this will be discussed in the following section, perhpas it is useful to note here that fractionation of a large quantum is pretty difficult in the conventional regime, and that this constraint is not so easy to satisfy for keV energy quanta.

7.6. Anomalous regime threshold energy

In the anomalous regime the threshold constraint can also be expressed in terms of an energy; we may write

$$\delta E^3 \;=\; \frac{\hbar\omega_0 \left(\mathbf{a}\cdot c\frac{d\mathbf{P}}{da}\right)^2 N_0^2}{4\times 10^{-4}} \;\geq\; (\Delta M c^2)^3. \tag{138}$$

The threshold energy is now

$$\delta E \;=\; 2500^{1/3}\,(\hbar\omega_0)^{1/3}\left(\mathbf{a}\cdot c\frac{d\mathbf{P}}{da}\right)^{2/3} N_0^{2/3}. \tag{139}$$

In the case of a monatomic crystal this becomes (again assuming alignment)

$$\delta E \;=\; 1250^{1/3}\,(Mc^2)^{1/3}|\mathbf{a}|^{2/3}(\hbar\omega_0)^{2/3}\left(\frac{N_0^2}{N}\right)^{1/3}. \tag{140}$$

We will see in the next section that this constraint is much easier to satisfy for keV quanta, and that we might understand collimated X-ray emission in the Karabut experiment in terms of a very similar constraint derived for the donor and receiver model.

7.7. Simple monatomic crystal threshold condition

If we adapt the general threshold condition above for a simple monatomic crystal, we find that it can be written in the form

$$4\times 10^{-4} \;\leq\; \frac{1}{4}\frac{1}{(\Delta n)^3}\;\times\;\begin{cases} n_0\dfrac{r}{\sqrt{1-r^2}}, & r<1, \\[2ex] \dfrac{1}{4}\left(\dfrac{N_0\Delta M c^2}{\hbar\omega_0}\right) r\sqrt{\dfrac{r^2-1}{r^2+1}}, & r>1, \end{cases} \tag{141}$$

where the ratio r is defined according to

$$r \;=\; 4|\mathbf{a}|^2\frac{Mc^2}{\Delta M c^2}\frac{N_0}{N}. \tag{142}$$

Before proceeding, we would like to draw attention to this version of the fractionation constraint for a number of reasons. The basic lossy spin–boson model under discussion is reasonably complicated, especially when we take into account

all three of the constraints; so to obtain an approximate version of the threshold constraint in such a simple form was unexpected. Additionally, we see that this threshold condition depends only on four basic parameters of the system: the number of phonons present n_0; the number of phonons Δn produced by the fractionation of the large quantum; the ratio r which depends on the **a** matrix element, and which determines whether the system is in the conventional or anomalous regime; and finally the number of virtual phonons

$$\frac{N_0 \Delta M c^2}{4\hbar\omega_0}.$$

We see from this that when r is less than unity, the system is in the conventional regime, and the threshold constraint becomes

$$\frac{1}{4}\frac{r}{(\Delta n)^3}\, n_0 \;\geq\; 4\times 10^{-4}, \qquad r \ll 1. \tag{143}$$

To reach the threshold in this regime, the number of phonons needs to be increased to satisfy

$$n_0 \;\geq\; 1.6\times 10^{-3}\frac{(\Delta n)^3}{r}, \qquad r \ll 1. \tag{144}$$

In the anomalous regime the threshold condition is

$$\frac{1}{4}\frac{r}{(\Delta n)^3}\left(\frac{N_0 \Delta M c^2}{4\hbar\omega_0}\right) \;\geq\; 4\times 10^{-4}, \qquad r \gg 1. \tag{145}$$

The threshold condition in the anomalous regime is similar in form to that of the conventional regime; we could write it in the form

$$\frac{1}{4}\frac{r}{(\Delta n)^3}\, n_V \;\geq\; 4\times 10^{-4}, \qquad r \gg 1, \tag{146}$$

where n_V is the number of virtual phonons

$$n_V \;=\; \frac{N_0 \Delta M c^2}{4\hbar\omega_0}. \tag{147}$$

The coupling between the phonons and excited nuclei result in the generation of a large number of virtual phonons in the anomalous regime, as well as a large number of virtual excited nuclei. Roughly a quarter of all of the nuclei involved in the transition are excited in the anomalous regime in this model.

8. Theory and the Karabut Experiment

Back in 1989 we understood that the observation of excess heat in the Fleischmann–Pons experiment [1,2] probably implied that a large MeV quantum was being fractionated into a great many small quanta. This provided us with the motivation to seek models capable of efficient coherent energy exchange under conditions of fractionation, leading ultimately to the lossy spin–boson model. However, it was collimated X-ray emission in the Karabut experiment [23–28], which we interpreted as showing direct conversion of vibration to nuclear energy, that motivated us to explore the new condensed matter model with relativistic coupling to internal nuclear degrees of freedom [29–31].

Once the new theory had gone through a preliminary development, we applied it to a model corresponding to our interpretation of the Karabut experiment, and found that the experimental conditions we estimated to be consistent with our interpretation were inconsistent with sufficient fractionation according to the model. This motivated us to seek stronger fractionation, first in the model of last summer [30] (which was found to be in error [31]), and then in fluctuations due to electron-phonon coupling [32] (which was found to be a small effect earlier in this paper). However, from the development of the previous sections we now understand that there can be a large enhancement in the fractionation power due to virtual phonon generation. This motivates us to revisit collimated X-ray emission in the Karabut experiment, to examine our earlier interpretation, and to suggest a new interpretation.

8.1. Fractionation by the 1565 eV transition in ^{201}Hg

Our earlier interpretation of the Karabut experiment focused on the 1565 eV transition in ^{201}Hg, which we proposed was present on the surface in small amounts. This transition is unique in that it is the lowest energy transition from a stable ground state nucleus. However, based on the discussion in the previous section, our attention is drawn to the fact that ^{201}Hg is present in the Karabut experiment as an impurity, so that

$$r \;=\; 4|\mathbf{a}|^2 \frac{Mc^2}{\Delta Mc^2}\frac{N_0}{N} \;\ll\; 1. \tag{148}$$

Although we do not have a value for the **a** matrix element in this case, we can quantify what value would be needed to reach the anomalous regime; $r = 1$ for an impurity level of 10 ppm (and optimistically assuming that all of the ^{201}Hg is initially in the same spin state) when $|\mathbf{a}|$ satisfies

$$|\mathbf{a}_{\rm thresh}| \;=\; \sqrt{\frac{1}{4}\frac{N}{N_0}\frac{\Delta Mc^2}{Mc^2}} \;\rightarrow\; \sqrt{\frac{1}{4}\left(\frac{1}{0.132\ 10^{-5}}\right)\left(\frac{1565\ {\rm eV}}{201\ {\rm amu}}\right)} \;=\; 0.04. \tag{149}$$

This seems much too high to be plausible, so we conclude that ^{201}Hg as an impurity would would fractionate in the conventional regime.

We can use the analysis of the previous section to determine what energy can be fractionated by the 1565 eV transition. Results are shown in Fig. 4. These results are interesting in the sense that we see threshold energies of more than 40 eV in the upper right corner, which is a highly nontrivial amount of fractionation power given that we are starting from $\hbar\omega_0 = 0.13$ μeV. On the other hand, clearly the transition is well short of the keV regime needed to be relevant to the experimental results. Our conclusion is that Hg on the surface or in the bulk as an impurity simply cannot fractionate a sufficiently large quantum to be relevant to the observed collimated X-ray emission. We note that there would be no problem with the 1565 eV transition being the source of the radiation as long as fractionation is accomplished on some other transition (e.g., in a donor and receiver type of model).

8.2. Fractionation in the anomalous regime

Let us consider briefly a different experiment intended to access the anomalous regime, where Hg is no longer an impurity. Suppose that we consider a difficult physics experiment in which a frozen sample of isotopically pure ^{201}Hg is initialized in a single nuclear spin state; the magnitude of the $|\mathbf{a}|$ matrix element needed to reach the anomalous regime in this case is

$$|\mathbf{a}_{\rm thresh}| \;=\; \sqrt{\frac{1}{4}\frac{N}{N_0}\frac{\Delta Mc^2}{Mc^2}} \;\rightarrow\; \sqrt{\frac{1}{4}\left(\frac{1565\ {\rm eV}}{201\ {\rm amu}}\right)} \;=\; 4.57\times 10^{-5}. \tag{150}$$

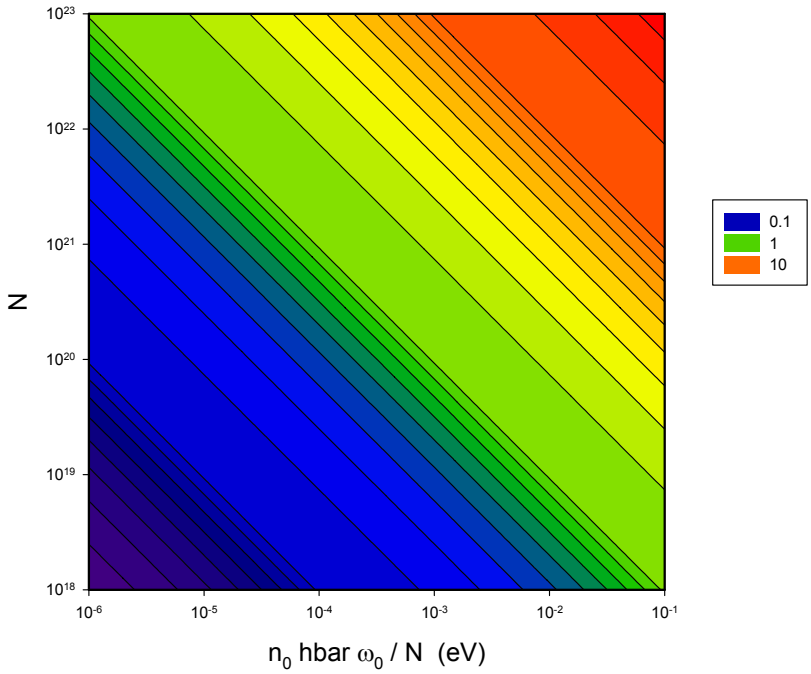

Figure 4. Threshold energy δE (eV) as a function of number of sample atoms and energy (eV) per atom; assumed for this calculation is $r = 10^{-6}$, a frequency $\omega_0/2\pi$ of 100 MHz, and a cathode material with a mass A close to 201.

As noted above the **a** matrix element is not known at present; however, it seems to us that it is likely to be larger than this threshold value.

The fractionation energy δE in this case is shown in Fig. 5. We see that the fractionation energy is independent of how highly excited the lattice is (keeping in mind that it must be highly excited for the model to be relevant in the first place), and that a fractionation energy in the vicinity of 1565 eV in this example requires about 5×10^{17} nuclei.

8.3. Fractionation on other low-energy transitions

We are motivated from the discussion above to consider other low-energy nuclear transitions that occur in some of the isotopes which are not impurities in the cathodes. Our attention turns immediately to the case of Nb, which gave positive results in Karabut's experiment. This element is interesting because it has only a single stable isotope (^{93}Nb), and there is an M4 transition to a low-energy metastable state at 30.77 keV (which is a candidate transition for fractionation). We can determine a constraint on the **a** matrix element to get into the anomalous regime

$$|\mathbf{a}_{\rm thresh}| = \sqrt{\frac{1}{4}\frac{N}{N_0}\frac{\Delta Mc^2}{Mc^2}} \rightarrow \sqrt{\frac{1}{4}(9)\left(\frac{30.77\ {\rm keV}}{93\ {\rm amu}}\right)} = 8.94 \times 10^{-4}, \tag{151}$$

where we note that the ground state has a spin of 9/2 (and we consider for this estimate that each sub-level transition

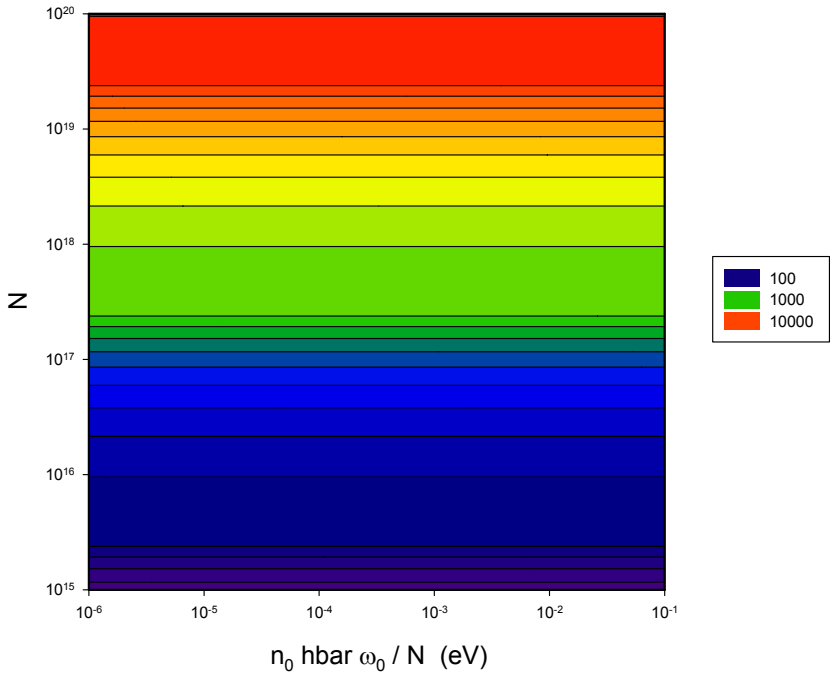

Figure 5. Threshold energy δE (eV) as a function of number of sample atoms and energy (eV) per atom; assumed for this calculation is $r = 2$, a frequency $\omega_0/2\pi$ of 100 MHz, and a cathode material with a mass A close to 201.

be considered independently). This threshold seems sufficiently low that there is a good chance that the 30.77 keV transition can exceed this value.

Let us suppose now that the 30.77 keV transition in ^{93}Nb can reach the anomalous regime; if so, then what kind of fractionation energy might we expect. Results are shown in Fig. 6. Since the longitudinal sound speed is 4.92×10^5 cm/s, a 25 μ thick cathode has a fundamental frequency at 98.4 MHz. For a cathode diameter of 1 cm, the total number of Nb atoms present is 1.1×10^{20}; if we assume that about half of these nuclei experience motion sufficiently uniform to be accounted for by a Dicke model, then we estimate N to be about 5.5×10^{19}. From Fig. 6 we see that the fractionation energy δE is about 5 keV. This fractionation energy is too low to support efficient excitation of the 30.77 keV transition (consistent with experiment). From data presented by Karabut, we see that X-ray emission is seen up to about 4 keV in Nb [28], which we would expect to be consistent with the threshold fractionation energy (although the X-rays would not be from the 30.77 keV transition). The relation between threshold fractionation energy and number of nuclei participating in the transition (once r has been fixed) in the anomalous regime is

$$\delta E = \left[\frac{1}{(16)(4 \times 10^{-4})} \, r \sqrt{\frac{r^2 - 1}{r^2 + 1}} N_0 \right]^{1/2} \hbar\omega_0. \tag{152}$$

There is an E3 transition to a metastable state in ^{103}Rh at 39.73 keV, which does not seem to be among the cathode

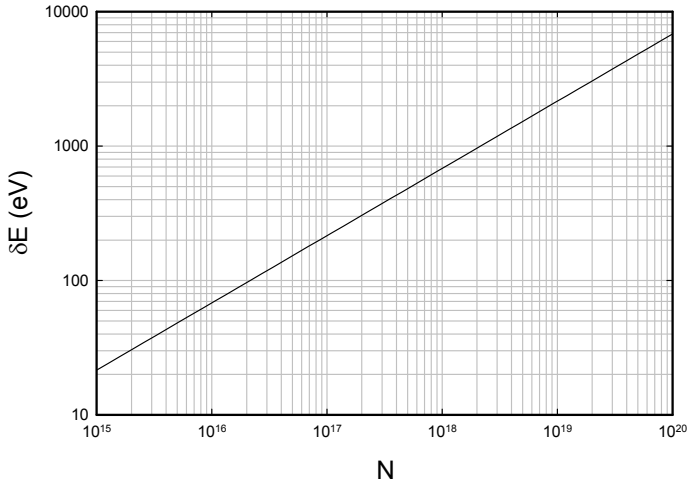

Figure 6. Threshold energy δE (eV) as a function of number of sample atoms and energy (eV) per atom; assumed for this calculation is $r = 2$, a frequency $\omega_0/2\pi$ of 100 MHz, and a cathode material made of Nb.

materials worked with by Karabut. A similar computation to what we did above leads to

$$|\mathbf{a}_{\rm thresh}| \;=\; \sqrt{\frac{1}{4}\frac{N}{N_0}\frac{\Delta Mc^2}{Mc^2}} \;\rightarrow\; \sqrt{\frac{1}{4}(2)\left(\frac{39.73\ {\rm keV}}{102\ {\rm amu}}\right)} \;=\; 4.57\times 10^{-4}. \tag{153}$$

This threshold **a** matrix value is even lower, and may be consistent with anomalous regime operation.

8.4. Donor and receiver model

We proposed the donor and receiver model [40] to account for fractionation in the case of excess heat production. In this model, the donor transition is assumed to be weakly coupled to the highly excited phonon mode, consistent with the weakness of the $D_2/^4$He transition on account of hindrance by the Coulomb barrier. Since the donor transition in this case is much too weak to fractionate a large quantum, we proposed that a second much stronger transition was present which would fractionate the large quantum in the donor and receiver model. Subsequently, we have noted that this model has wider applicability to any situation where strong and weak transitions are coupled to the same highly excited phonon mode.

In light of the discussion above, we are motivated to apply the model to lattice-induced excitation in the Karabut experiment. The weakly coupled transition in this case is the 1565 eV transition in ^{201}Hg present as an impurity. The strongly coupled transition is as yet unidentified, except perhaps in the case of ^{93}Nb where we can identify a plausible candidate. However, we can take advantage of an important feature of the models described above; if a transition makes it into the anomalous regime, then the response is pretty much fixed independent of the details of the transition. We can make use of this in an examination of the donor and receiver model with a receiver transition assumed to be in the anomalous regime.

From previous work, we know that the indirect coupling matrix element for the weakly coupled transition can be written as

$$\frac{V_1^{\rm eff}}{(\Delta Mc^2)_1} = 2g_1|\langle v_n|v_{n+\Delta n}\rangle_2| = 2\frac{\left(\mathbf{a}_1\cdot c\frac{{\rm d}\mathbf{P}}{{\rm d}a}\right)\sqrt{n}\sqrt{S_1^2-m_1^2}}{(\Delta Mc^2)_1}|\langle v_n|v_{n+\Delta n_1}\rangle_2|. \quad (154)$$

The indirect coupling matrix element is determined by the dimensionless coupling parameter associated with the weak transition, and an overlap matrix element that depends on the strongly coupled transition. This overlap matrix element serves as a hindrance factor that depends on the ability of the strongly coupled transition to fractionate the large quantum associated with the receiver transition.

In the pulse and amplitude approximation [39] we can use the pulse to approximate

$$|\langle v_n|v_{n+\Delta n_1}\rangle_2| \rightarrow |\langle u_n|u_{u+\Delta n_1}\rangle_2|. \quad (155)$$

If we further make a continuum approximation, then

$$|\langle u_n|u_{u+\Delta n_1}\rangle_2| \rightarrow \left|\left\langle u(z)\middle|u\left(z+\frac{\Delta n_1}{\Delta n_2}\right)\right\rangle_2\right|. \quad (156)$$

Since the continuous $u(z)$ are well approximated by Airy functions, we can evaluate the overlap matrix element using [38]

$$\left|\left\langle u(z)\middle|u\left(z+\frac{\Delta n_1}{\Delta n_2}\right)\right\rangle_2\right| \rightarrow f\left(\frac{\Delta n_1}{(2g_u)_2^{1/3}}\right), \quad (157)$$

where the function $f(y)$ is defined according to

$$f(y) = \frac{\int_{-2.33810}^{\infty}{\rm Ai}(x){\rm Ai}(x+y){\rm d}x}{\int_{-2.33810}^{\infty}{\rm Ai}^2(x){\rm d}x}. \quad (158)$$

This function is illustrated in Fig. 7.

As before, it seems useful to define a threshold fractionation energy for the strongly coupled transition. We might adopt a constraint of the form

$$\frac{\Delta n_1}{(2g_u)_2^{1/3}} \leq 10. \quad (159)$$

This can be compared to the constraint above for lattice-induced nuclear excitation, which can be recast as

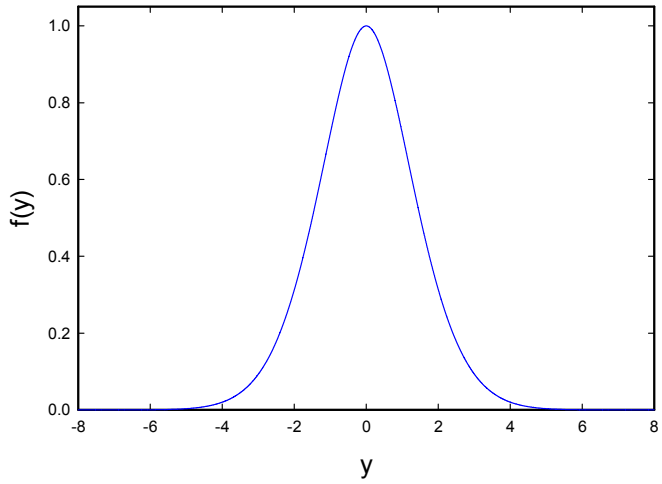

Figure 7. Plot of $f(y)$ as a function of y.

$$\frac{\Delta n}{(2g_u)^{1/3}} \leq \left(\frac{1}{4\times 10^{-4}}\right)^{1/3} = 13.57. \tag{160}$$

We see from this that the fractionation threshold energy for a transition in lattice-induced nuclear excitation is essentially the same fractionation threshold energy when it serves as the strongly coupled transition in a donor and receiver scheme.

We can rewrite the donor and receiver constraint assuming that the strongly coupled transition is in the anomalous regime using

$$(g_u)_2 = \frac{\left(\mathbf{a}_2\cdot c\frac{\mathrm{d}\,\mathbf{P}}{\mathrm{d}a}\right)\left\langle\sqrt{S_2^2-m_2^2}\langle\sqrt{n}\rangle\right\rangle}{\hbar\omega_0}. \tag{161}$$

In the anomalous regime we can write

$$\begin{aligned}\left\langle\sqrt{S^2-m^2}\langle\sqrt{n}\rangle\right\rangle &\rightarrow \frac{1}{4}\sqrt{n_0N_0}\frac{N_0}{\sqrt{N_c}}\sqrt{\frac{1-\left(\frac{\sqrt{N_c}}{4\gamma_d}\right)^2}{1+\left(\frac{\sqrt{N_c}}{4\gamma_d}\right)^2}}\\ &= \frac{\sqrt{n_0}N_0^{3/2}}{16\gamma_d}r\sqrt{\frac{r^2-1}{r^2+1}},\end{aligned} \tag{162}$$

which leads to

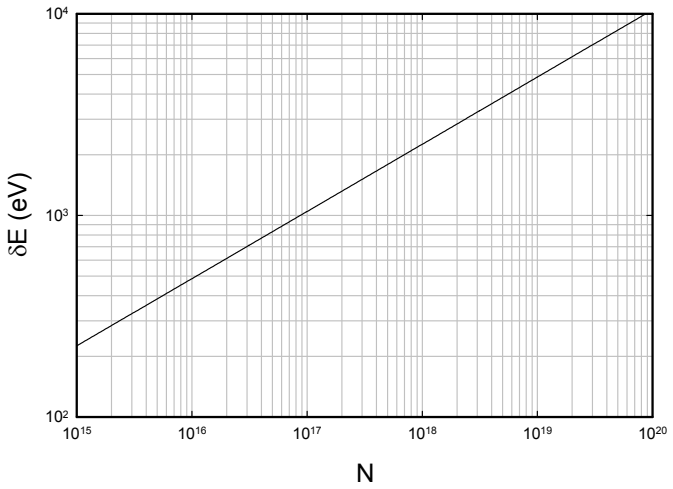

Figure 8. Threshold energy δE (eV) for a donor and receiver model, with the 30.77 keV transition in ^{93}Nb as the strongly coupled transition, and the 1565 eV transition in ^{201}Hg as the weakly coupled transition, as a function of number of sample atoms and energy (eV) per atom; assumed for this calculation is $r = 2$, a frequency $\omega_0/2\pi$ of 100 MHz, and a cathode material made of Nb (with Hg as an impurity).

$$(g_u)_2 \;\rightarrow\; \frac{1}{16}\left(\frac{\Delta Mc^2}{\hbar\omega_0}N_0 r\sqrt{\frac{r^2-1}{r^2+1}}\right)_2, \qquad r_2 > 1. \tag{163}$$

We can use this to recast the threshold constraint for transitions on the weakly coupled system in terms of a threshold fractionation energy

$$\delta E \;=\; 5\left(\frac{\Delta Mc^2}{\hbar\omega_0}N_0 r\sqrt{\frac{r^2-1}{r^2+1}}\right)_2^{1/3}\hbar\omega_0 \;\geq\; (\Delta Mc^2)_1. \tag{164}$$

This constraint is illustrated in Fig. 8. We see that the threshold for excitation of the ^{201}Hg transition is about 3×10^{17} Nb atoms.

The models considered so far have primarily been concerned with coherent dynamics, but there should be no difficulty extending them slightly for excitation of the ^{201}Hg transition and subsequent superradiant decay. In this case, the energy transferred from the strongly coupled transition could go into exciting the ^{201}Hg 1565 eV transition off of resonance, with the total transferred energy emitted as an X-ray. The same constraints should apply in this case as well, so that collimated X-ray radiation up to a few keV would be expected, consistent with experiment [28].

9. Summary and Conclusions

As outlined in the Introduction and in subsequent sections, the Fleischmann–Pons experiment motivated us to consider mechanisms through which a large quantum could be fractionated, and led to the lossy spin–boson model and the

generalization to the donor and receiver model. Similarly, collimated X-rays in the Karabut experiment motivated us to seek stronger coupling between vibrational and nuclear degrees of freedom, which led to the new relativistic theory under discussion in this work.

Once we had the new relativistic theory, we had expected it to make sense out of the Karabut experiment and other anomalies. However, when we applied it to our interpretation of the Karabut experiment, the results were discouraging. This led to an effort last year to seek an enhancement of the fractionation effect due to coupling with very strong static transitions, resulting in a model that agreed reasonably well with experiment but contained an internal error. This also led to a substantial effort to include phonon fluctuations due to coupling with conduction electrons in metals. We found in this work that phonon fluctuations from the Bloch model are small compared to phonon fluctuations induced by phonon–nuclear coupling on dynamic transitions.

All of this brought us back to reconsider the basic model once more, this time more systematically than in previous work. The analyses of early last year focused on using the pulse and amplitude approximation on the phonon distribution in the local approximation, and did not lead to agreement with experiment. In this work we described the associated models in more detail than was done in previous publications. However, this time we considered a self-consistent model for the nuclear excited state distribution, including the possibility that the number of virtual phonons might be large. Although we had constructed models for the nuclear excited state distribution previously, we had not imagined that so many virtual phonons might be present.

This new self-consistent model for the nuclear excited state distribution showed clearly that there are two basic regimes. In the conventional regime, the excited state distribution closely resembles what one would obtain with simple static coupling. The fractionation of a large quantum in the conventional regime is difficult in the sense that a large number of nuclei are needed, and the system has to be driven very hard. In the anomalous regime, the number of virtual phonons can exceed the number of real phonons, and the increased coupling strength that results from these additional phonons has a profound impact on the nuclear excited state distribution. The fractionation of a large quantum in the anomalous regime is very much easier, and depends on the number of nuclei present and the mode frequency. Since the number of virtual phonons in this regime can be large, fractionation becomes independent of the number of real phonons (except that enough must be present for the highly excited mode to avoid interference from all the other modes).

With this new analysis, we returned once again to the problem of collimated X-ray emission in the Karabut experiment. In earlier work we had interpreted the experiment (erroneously) as showing coherent energy exchange between vibrations and nuclear excitation due to fractionation on the 1565 eV transition in ^{201}Hg as an impurity. As discussed above, a transition in an impurity at low concentration is most like going to fall into the conventional regime, and we find (as we have found before) that the fractionation strength of the 1565 eV transition is just too low to be relevant to the experimental results. However, a frozen mercury sample with enough ^{201}Hg nuclei initialized in the same nuclear spin state would very likely make it into the anomalous regime. Vibrational excitation in the 100 MHz regime of the fundamental resonance of a thin sample would be a very interesting, although perhaps technically challenging.

We applied the model to the 30.77 keV transition in ^{93}Nb, and developed a constraint on the **a** matrix element for the system to be in the anomalous regime; our conclusion from this is that there is a substantial likelihood that the transition can make it. If so, the question is whether coherent dynamics would be expected under the conditions of the Karabut experiment. We concluded that the threshold fractionation energy in this case is lower than what would be needed, which is consistent with the absence of strong collimated emission at 30.77 keV in the experiment.

On the other hand, if the 30.77 keV transition can operate in the anomalous regime, then one would expect it to be able to fractionate large quanta to support coherent dynamics on the 1565 eV transition, in a donor and receiver model. The threshold fractionation energy for lattice-induced nuclear excitation is pretty much the same as for fractionation in a donor and receiver model (as expected since the hard part of both models is the fractionation of the same quantum), so while the 30.77 keV transition may not be able to fractionate a 30.77 keV quantum in the Karabut experiment, it should be able to fractionate large quanta up to about 5 keV. This corresponds well to the nearly 4 keV quanta observed

in collimated emission with a Nb cathode by Karabut.

Karabut sees collimated emission with a variety of different metal cathodes. In all cases, we would expect the 1565 eV ^{201}Hg transition to be on the receiving end of the converted vibrational energy in a donor and receiver kind of model, present as an uncontrolled impurity at low levels. However, in these cases we do not have an identification of the strongly coupled transition in the host cathode lattice. Since the fractionation energy depends weakly on the details of the transition once the system is in the anomalous regime, we have some ability to apply the model in these cases. Perhaps the biggest implication is that for the collimated emission to occur, there must be at least one transition that operates in the anomalous regime (even if we don't know which transition). Karabut's experiment interpreted in this way provides the important result that many metals have such transitions, suggesting that they are reasonably common. It will remain for future work to develop estimates for **a** matrix element from nuclear structure models. However, if controlled experiments can be developed that show collimated X-ray emission, then we should be able to extract equivalent information directly from experiment.

To date **a** matrix elements have been calculated for transitions in the deuteron [41], and for the $D_2/^4$He transition [42]. In the case of the deuteron transition, the magnitude of the **a** matrix element was estimated to be about 3×10^{-3}, which is too small for anomalous regime operation, since

$$r \;=\; 4|\mathbf{a}|^2 \frac{Mc^2}{\Delta Mc^2}\frac{N_0}{N} \;\rightarrow\; 4(3\times 10^{-3})^2 \left(\frac{2\text{ amu}}{127\text{ MeV}}\right)\left(\frac{1}{3}\right) \;=\; 1.76\times 10^{-4}. \tag{165}$$

However, it may be that the **a** matrix element in this case might be too low, since in the computation it was presumed that the proton and neutron act as Dirac particles (for the reduction of the $\boldsymbol{\alpha}$ matrices). We know that the proton and neutron are instead composites (and not Dirac particles), and that we should probably take this into account in calculating the **a** matrix element. To be philosophically consistent with our fundamental Hamiltonian of Eq. (1), perhaps we should think instead of a model for the deuteron based instead on

$$\hat{H} \;=\; \mathbf{M}_n c^2 + \mathbf{a}_n \cdot c\hat{\mathbf{P}}_n + \mathbf{M}_p c^2 + \mathbf{a}_p \cdot c\hat{\mathbf{P}}_p + \hat{V}_{np}. \tag{166}$$

One motivation for such a consideration is that excess heat in the Fleischmann–Pons model would seem to make sense if transitions in the deuteron could fractionate the large quantum. We might expect an increase on the general order of the ratio of the proton to quark mass, which might be sufficient to allow the system to make it into the anomalous regime. One wonders where transitions to negative energy states might be relevant, as long as real transitions are not allowed (there should be no problem with virtual transitions).

More relevant to the discussion in this paper is the issue of how the different elements used by Karabut might fractionate in the anomalous regime, since for most there are not obvious low-energy transitions available. Based on our experience with the deuteron, we know that it is problematic to develop a large **a** matrix element; yet, if our new interpretation of the Karabut experiment is correct, then somehow this it is not a rare occurrence. To address this issue systematically, we would imagine making use of a nuclear model based on

$$\hat{H} \;=\; \sum_j \left(\mathbf{M}c^2 + \mathbf{a}\cdot c\hat{\mathbf{P}}\right)_j + \sum_{j<k} \hat{V}_{jk}. \tag{167}$$

Although easily stated, the development of such models would take considerable effort.

Although we have not pursued the issue in this work, we note that the scaling laws are very favorable for fractionation with smaller number of nuclei in the THz regime, which is where we think that fractionation occurs in the Fleischmann–Pons experiment.

References

[1] M. Fleischmann, S. Pons and M. Hawkins, *J. Electroanal Chem.* **201** (1989) 301; errata **263** (1990) 187.

[2] M. Fleischmann, S. Pons, M.W. Anderson, L.J. Li and M. Hawkins, *J. Electroanal. Chem.* **287** (1990) 293.

[3] E. Storms, *Science of Low Energy Nuclear Reaction: A Comprehensive Compilation of Evidence and Explanations about Cold Fusion*, World Scientific, New Jersey, 2004.

[4] B.F. Bush, J.J. Lagowski, M.H. Miles and G.S. Ostrom, Helium production during the electrolysis of D_2O in cold fusion, *J. Electroanal. Chem.* **304** (1991) 271.

[5] M.H. Miles and B. Bush, Search for anomalous effects during D_2O Electrolysis using palladium cathodes, *Proc. ICCF3* (1992) 189.

[6] M.H. Miles, R.A. Hollins, B.F. Bush, J.J. Logowski and R.E. Miles, Correlation of excess power and helium production during D_2O and H_2O electrolysis using palladium cathodes, *J. Electroanal. Chem.* **346** (1993) 99.

[7] M.H. Miles, B. Bush and J.J. Lagowski, Anomalous effects involving excess power, radiation and helium production during D_2O electrolysis using palladium cathodes, *Fusion Technol.* **25** (1994) 478.

[8] P.L. Hagelstein, M.C.H. McKubre, D.J. Nagel, T.A. Chubb and R.J. Hekman, New physical effects in metal deuterides, *Proc. ICCF11* (2004) 23.

[9] P.L. Hagelstein, Constraints on energetic particles in the Fleischmann– Pons experiment, *Naturwissenschaften* 97 (2010) 345.

[10] F. Bloch and A. Siegert, Magnetic resonance for nonrotating fields, *Phys. Rev.* **57** (1940) 522.

[11] J. Shirley, Solution of the Schrödinger equation with a Hamiltonian periodic in time, *Phys. Rev.* **138** (1965) B979.

[12] C. Cohen-Tannoudji, J. Dupont-Roc and C. Fabre, A quantum calculation of the higher order terms in the Bloch–Siegert shift, *J. Phys. B: Atom. Molec. Phys.* **6** (1973) L214.

[13] P.L. Hagelstein and I.U. Chaudhary, Level splitting in association with the multiphoton Bloch-–Siegert shift, *J. Phys. B: At. Mol. Phys.* **41** (2008) 035601.

[14] P.L. Hagelstein and I.U. Chaudhary, Models relevant to excess heat production in Fleischmann–Pons experiments, *Low-energy nuclear reactions sourcebook* ACS Symp. Ser. **998** (2008) 249.

[15] P.L. Hagelstein, A unified model for anomalies in metal deuterides, *Proc. ICCF9* (2002) 121.

[16] P.L. Hagelstein and I.U. Chaudhary, Energy exchange in the lossy spin–boson model, *J. Cond. Mat. Nucl. Sci.* **5** (2011) 52.

[17] H. Feshbach, A unified theory of nuclear reactions, II *Ann. Phys.* **19** (1962) 287.

[18] P.L. Hagelstein and I.U. Chaudhary, Second-order formulation and scaling in the lossy spin–boson model, *J. Cond. Mat. Nucl. Sci.* **5** (2011) 87.

[19] P.L. Hagelstein and I.U. Chaudhary, Local approximation for the lossy spin-–boson model, *J. Cond. Mat. Nucl. Sci.* **5** (2011) 102.

[20] P.L. Hagelstein and I.U. Chaudhary, Coherent energy exchange in the strong coupling limit of the lossy spin–boson model, *J. Cond. Mat. Nucl. Sci.* **5** (2011) 116.

[21] P.L. Hagelstein and I.U. Chaudhary, Errata and comments on a recent set of papers in *J. Condensed Matter in Nucl. Sci.*, *J. Cond. Mat. Nucl. Sci.* **7** (2012) 1.

[22] P.L. Hagelstein, Bird's eye view of phonon models for excess heat in the Fleischmann–Pons experiment, *J. Cond. Mat. Nucl. Sci.* **6** (2011) 169.

[23] A.B. Karabut, Research into powerful solid X-ray laser (wave length is 0.8-1.2nm) with excitation of high current glow discharge ions, *Proc. 11th Int. Conf. on Emerging Nuclear Energy Systems*, 29 September–4 October 2002, Albuquerque, New Mexico, USA, pp. 374–381.

[24] A.B. Karabut, Experimental research into characteristics of X-ray emission from solid-state cathode medium of high-current glow Discharge, *Proc. 10th Int. Conf. on Cold Fusion*, August 24–29, 2003, Cambridge, MA, USA.

[25] A.B. Karabut, Research into characteristics of X-ray emission laser beams from solid-state cathode medium of high current glow discharge, *Proc. 11th Int. Conf. on Cold Fusion*, 31 October-–5 November, France, 2004, pp. 253–257.

[26] A.B. Karabut, Study of energetic and temporal characteristics of x-ray emission from solid state cathode medium of high current glow discharge, *Proc. 12th Int. Conf. on Cold Fusion*, December 2-–7, 2006, Japan, pp. 344-–350.

[27] A.B. Karabut, E.A. Karabut, Research into energy spectra of X-ray emission from solid cathode medium during the high current glow discharge operation and after the glow discharge current switch off, *Proc. 14th Int. Conf. on Cold Fusion*, August

10-–15, 2008, USA.
[28] A.B. Karabut, E.A. Karabut and P.L. Hagelstein, Spectral and temporal characteristics of X-ray emission from metal electrodes in a high-current glow discharge, *J. Cond. Mat. Nucl. Sci.* **6** (2012) 217.
[29] P.L. Hagelstein and I.U. Chaudhary, Including nuclear degrees of freedom in a lattice Hamiltonian, *J. Cond. Mat. Nucl. Sci.* **7** (2011) 35.
[30] P.L. Hagelstein and I.U. Chaudhary, A model for collimated emission in the Karabut experiment, *Proc. ICCF17* (in press).
[31] P.L. Hagelstein and I.U. Chaudhary, Phonon–nuclear coupling for anomalies in condensed matter nuclear science, *J. Cond. Mat. Nucl. Sci.*, submitted.
[32] P.L. Hagelstein and I.U. Chaudhary, Born–Oppenheimer and fixed-point models for second-order phonon exchange in a metal, *J. Cond. Mat. Nucl. Sci.*, submitted.
[33] J.M. Ziman, The electron-phonon interaction, according to the adiabatic approximation, *Math. Proc. Cambridge Philosophical Soc.* **51** (1955) 707.
[34] J.C. Taylor, The electron–phonon interaction, according to the adiabatic approximation, *Math. Proc. Cambridge Philosophical Soc.* **52** (1956) 693.
[35] L.J. Sham and J.M. Ziman, The electron–phonon interaction, *Solid State Phys.* **15** (1963) 221.
[36] S.K. Joshi and A.K. Rajagopa, Lattice dynamics of metals, *Solid State Phys.* **22** 159 (1969).
[37] G. Mahan, *Many-Particle Physics*, Plenum Press, New York, 1990.
[38] P.L. Hagelstein and I.U. Chaudhary, Lossy spin-–boson model with an unstable upper state and extension to N-level systems, *J. Cond. Mat. Nucl. Sci.* **11** 59 (2013).
[39] P.L. Hagelstein and I.U. Chaudhary, Pulse and amplitude approximation for the lossy spin–boson model, *J. Cond. Mat. Nucl. Sci.* **9** 30 (2012).
[40] P.L. Hagelstein and I.U. Chaudhary, Generalization of the lossy spin-–boson model to donor and receiver systems, *J. Cond. Mat. Nucl. Sci.* **5** 140 (2011).
[41] P.L. Hagelstein and I.U. Chaudhary, Coupling between a deuteron and a lattice, *J. Cond. Mat. Nucl. Sci.* **9** 50 (2012).
[42] P.L. Hagelstein and I.U. Chaudhary, Central and tensor contributions to the phonon-exchange matrix element for the $D_2/^4He$ transition, *J. Cond. Mat. Nucl. Sci.* **11** 15 (2013).